Pathfinder Mission

for

Climate Absolute Radiance and Refractivity Observatory (CLARREO)

Mission Scientist: Bruce A. Wielicki[1]

Project Scientist: Rosemary R. Baize[1]

Project Manager: Gary A. Fleming[1]

Science Team:

D. F. Young[1], M. G. Mlynczak[1], K. J. Thome[2], S. Leroy[3], C. O. Ao[4], R. Bantges[5], F. Best[6], H. Brindley[5], J. Butler[2], M. Bynum[7], R. Cageao[1], W. Collins[8], R. Cooke[15], J. Corliss[1],J.C. Currey[1], J.A. Dykema[3], D.R. Doelling[1], B. Dunn[1], D. R. Feldman[8], D. Goldin[11], R. Holz[6], X. Huang[9], Y. Huang[10], D. Jennings[2], Z. Jin[11], D.G. Johnson[1], S. Kato[1], R. Knuteson[6], G. Kopp[12], D.P. Kratz[1], J. Leckey[1], X. Liu[1], C. Lukashin[1], A. Lyapustin[2], A. J. Mannucci[4], J. McCorkel[2], P. Pilewskie[12], H. Revercomb[6], J. Rice[13], C. M. Roithmayr[1], F. Rose[11], Y. L. Shea[1], W. L. Smith, Sr.[6], B. Soden[14], P. W. Speth[1], T. C. Stone[16], W. Sun[11], D. Tobin[6], X. Xiong[2]

Editor-in-Chief: Yolanda L. Shea[1]

Affiliations

1. NASA Langley Research Center, Hampton, VA
2. NASA Goddard Space Flight Center, Greenbelt, MD
3. Harvard University, Cambridge, MA
4. Jet Propulsion Laboratory, Pasadena, CA
5. Imperial College, London, UK
6. University of Wisconsin, Madison, WI
7. Analytical Mechanics Associates Inc., Hampton, VA
8. Lawrence Berkeley National Laboratory, Berkeley, CA
9. University of Michigan, Ann Arbor, MI
10. McGill University, Montreal, Quebec, Canada
11. Science Systems and Applications, Inc., Hampton, VA
12. University of Colorado, Boulder, CO
13. National Institute of Standards and Technology, Gaithersburg, MD
14. University of Miami, Miami, FL
15. Resources for the Future, Washington, DC
16. US Geological Survey, Flagstaff, AZ

Executive Summary

The Pathfinder for the Climate Absolute Radiance and Refractivity Observatory (CLARREO), or CLARREO Pathfinder (CPF), is a cost-capped NASA directed mission for demonstration of key technologies necessary for the full CLARREO mission. CLARREO is a Tier 1 mission recommended by the 2007 NRC Earth Science Decadal Survey. The CLARREO mission's primary objective is to produce highly accurate climate records to test climate projections in order to improve climate models and ultimately enable sound policy decisions. This objective is accomplished through accurate decadal satellite observations traceable to the Système international d'unités (SI units) that are sensitive to key climate variables, including climate feedbacks, responses, and radiative forcings. Uncertainties in such climate variables drive current climate model projection uncertainties.

In 2016, funds were appropriated for a Pathfinder mission, to demonstrate essential measurement technologies required for the full CLARREO mission. These funds support the development and flight of a Reflected Solar (RS) spectrometer to be hosted on the International Space Station (ISS) in the 2020 timeframe. The CLARREO Pathfinder is a Class D mission that includes one year of operations on the ISS and one additional year for the analysis of acquired data.

CPF will provide highly accurate spectral reflectance measurements enabled by a RS spectrometer operating between 350 nm and 2300 nm (> 95% of reflected solar energy) with continuous spectral coverage with a broadband uncertainty < 0.5% and spectral uncertainty < 1% (k=2)[1]. The RS spectrometer will be capable of pointing to the sun and moon for calibration, as well as tracking time, space, and angle-matched observations when used during reference inter-calibration of other operational sensors. The CPF will be mounted on the ExPRESS logistics carrier (ELC-1), an external attached payload platform on the ISS, for nadir Earth observations between 52°N and 52°S latitude with full sampling of the diurnal cycle obtained approximately monthly.

CPF will reduce risks for the full CLARREO mission by demonstrating high absolute accuracy, SI-traceable, on-orbit calibration approaches and by demonstrating high-accuracy reference inter-calibration with other operational satellite instruments (e.g. Clouds and the Earth's Radiant Energy System – CERES, Visible Infrared Imaging Radiometer Suite – VIIRS). Lessons learned from CLARREO Pathfinder will provide benefits to many other NASA Earth Science Missions including the following: 1) Improved laboratory SI-traceable calibration approaches, 2) Development and testing of innovative on-orbit SI-traceable calibration methods, 3) Inter-calibration of key sensors operational during the CPF lifetime, and an 4) Improved lunar spectral irradiance calibration standard.

[1] We use the general coverage factor k; $k = 2$ means a 95% confidence level (2σ) for a Gaussian distribution.

Contents

1 Introduction

In its 2007 Earth Science and Applications Decadal Survey, the National Research Council recommended the Climate Absolute Radiance and Refractivity Observatory (CLARREO) mission to address the critical issue of the lack of sufficient absolute accuracy for many current climate change observations to confidently observe the small but critical climate change signals over decadal time scales [*National Research Council*, 2007]. Observing decadal climate change is critical to assessing the accuracy of climate model projections and physically attributing observed climate changes [*Stocker et al.*, 2013, *Masson and Knutti*, 2011, *Stott and Kettleborough*, 2002]. Sound policymaking requires high confidence in climate predictions that have been verified against decadal change observations with well-known, rigorous accuracy requirements. Concerns about satellite data accuracy and the need for improvements have been expressed in U.S. interagency climate satellite calibration reports [*Ohring et al.*, 2005, 2007] and international climate observation system plans including the Global Earth Observing System of Systems plan [*Lautenbacher Jr*, 2005], the Global Climate Observing System Implementation Plan [*GCOS-154*, 2011], and the Global Space Based Inter-calibration System plan [*Goldberg*, 2007]. Common challenges with current satellite observations expressed in these documents include uncertain long-term drifts in calibration, absolute accuracy lower than typical decadal change signals, and the inability to observe decadal climate change with resiliency to gaps in observations.

The CLARREO mission addresses these concerns by providing an unprecedented level of absolute accuracy in global satellite observations that can be traced to international physical standards such as the SI standards for the second, the Kelvin, and the Watt [*Wielicki et al.*, 2013]. The CLARREO objectives of higher accuracy for decadal change observations lead to a unique set of observing strategies compared to those employed in previous satellite missions, especially those designed to observe weather or climate processes. The required measurement accuracy levels are determined by the projected large spatial (zonal, global) and long temporal (seasonal, annual, decadal) changes in key climate parameters and the background natural variability above which such changes must be detected. CLARREO requirements are therefore based on the absolute accuracy needed to detect decadal climate changes rather than instantaneous instrument noise levels. The result is the creation of climate change benchmark measurements defined by three fundamental characteristics:

1. Traceable to fundamental SI standards and robust to gaps in the measurement record;
2. Sufficient time/space/angle sampling to reduce aliasing bias errors in global decadal change observations to well below predicted decadal climate change and below natural climate variability; and
3. Sufficient information content to be sensitive to changes in key climate change variables.

The climate benchmarks to be provided by CLARREO were defined in the NRC Decadal Survey to include three types of observations:

1. Spectrally resolved infrared (IR) radiance emitted from Earth to space measured with

an accuracy of 0.07 K (k = 2)[2], traceable to the SI standard for thermodynamic temperature measured in degrees Kelvin.

2. Spectrally resolved reflected solar (RS) nadir reflectance with an accuracy of 0.3% (k = 2). The percentage is relative to the mean spectral reflectance of the Earth of about 0.3. While spectral reflectance is a measurement relative to solar spectral irradiance, use of the spectral solar irradiance observations made by the Total Solar Irradiance Spectrometer (TSIS) enables traceability to the SI standard for power measured in Watts.

3. Observations by Global Navigation Satellite Systems – Radio Occultation (GNSS-RO) instruments. The GNSS-RO benchmark measurement is the phase delay rate of the transmitted RO signal occulted by the atmosphere from low Earth orbit (LEO) with an accuracy of 0.06% (k = 2) for a range of altitudes from 5 to 20 km in the atmosphere and is traceable to the SI standard for time measured in seconds.

The CLARREO IR, RS, and RO observations were designed to provide information on the most critical but least understood climate forcings, responses, and feedbacks associated with the vertical distribution of atmospheric temperature and water vapor (IR/RS/RO), broadband reflected (RS) and emitted (IR) irradiance, cloud properties (IR/RS), surface albedo (RS), temperature (IR), and emissivity (IR). These measurements were to be used to achieve three independent CLARREO mission goals [*National Research Council*, 2007]:

1. unambiguously documenting changes in the climate system;
2. testing and improving forecasts of future climate change; and
3. improving the accuracy of existing climate and weather sensors by providing SI-traceable reference spectrometers in orbit.

The NASA FY2016 President's Budget request included funds for a CLARREO Pathfinder (CPF), a technology demonstration to be launched to the International Space Station (ISS) in the 2020 timeframe that will serve as a risk reduction for the full 2007 Decadal Survey-recommended CLARREO mission. The guidance in the budget request stated that the CLARREO Pathfinder was to demonstrate the capability of essential measurement technologies for the full CLARREO mission, validate the high-accuracy calibration requirements needed for climate change studies, and initiate climate benchmark measurements. With the passage of the FY2016 Federal Budget, the NASA Science Mission Directorate, Earth Science Division (ESD) provided approval to proceed with a CLARREO Pathfinder mission to the ISS. The appropriated funds for CLARREO Pathfinder support the development and launch of a Reflected Solar spectrometer, one year of operations for this instrument on the ISS, and one additional year of analysis of the data acquired. The NASA Risk Classification assigned to the CLARREO Pathfinder is Class D per NASA Procedural Requirements (NPR) 8705.4. With the RS spectrometer, it is anticipated that CLARREO Pathfinder will

[2] We use the general coverage factor k to establish a more rigorous tie between the climate science and metrology research communities. For a Gaussian distribution, k = 2 is equivalent to a 95% confidence level (i.e. 2σ).

demonstrate unprecedented on-orbit SI-traceable accuracy in reflectance measurements (see Section 4.1).

Lessons learned from CLARREO Pathfinder will benefit future CLARREO-like missions. CPF, as a technology demonstration of only the Reflected Solar portion of CLARREO, is not the full Decadal Survey-recommended CLARREO mission (see Section 3.2). Rather, the objective of CPF is to reduce risk and demonstrate new capabilities that a future full CLARREO mission will provide once operational. Specifically, the CPF will demonstrate high accuracy calibration approaches and show that such high accuracy SI-traceability can be maintained in orbit. Additionally, CPF will show that high accuracy in-orbit inter-calibration is achievable with a demonstration that will include a subset of the instruments for which CLARREO could serve as an in-orbit calibration standard. In addition to the benefits that CPF provides to a future full CLARREO mission, the lessons learned from CPF will also benefit other NASA Earth Science missions. These benefits include improved laboratory calibration approaches, the development and testing of innovative on-orbit SI-traceable methods for RS instruments, the transfer of calibration to sensors concurrently operational with CPF, and the provision of an improved lunar irradiance standard.

2 CLARREO Pathfinder Science Objectives

The science value of the full CLARREO mission [*National Research Council*, 2007, *Wielicki et al.*, 2013] has been determined in terms of decadal change in climate forcings, feedbacks, and responses relevant to the information content in RS and IR spectra and RO observations. Additionally, its science value has been based upon its contribution as a reference inter-calibration standard for IR and RS satellite sensors. Mission requirements for the full CLARREO mission were determined such that the mission would be able to detect decadal change of some of the most important elements of the climate system: temperature, water vapor, cloud properties, TOA (top-of-atmosphere) irradiance, and surface properties (e.g. albedo). Decadal change observations from the full CLARREO mission are also key to reducing uncertainties in the climate feedbacks that drive uncertainty in climate sensitivity. Measurements from the full CLARREO mission will help quantify radiative forcing from anthropogenic changes in land albedo, will confirm the effect of greenhouse gases on infrared emissions to space, and will make modest contributions to aerosol direct radiative forcing.

Most of the global satellite data sets, which tend to be designed to focus on climate process studies, are not yet sufficiently accurate to test the small, albeit critical, signals of decadal change. Accuracy requirements are less stringent for climate process studies than for climate trend studies. The CLARREO mission has been designed to address this need in the climate observing system by establishing, for the first time, satellite observations with sufficiently high accuracy that provides sensitivity to decadal changes.

The full CLARREO mission rely on metrology advances made in the past decade to provide significant improvements in the calibration of RS and IR and on the advances in using RO to

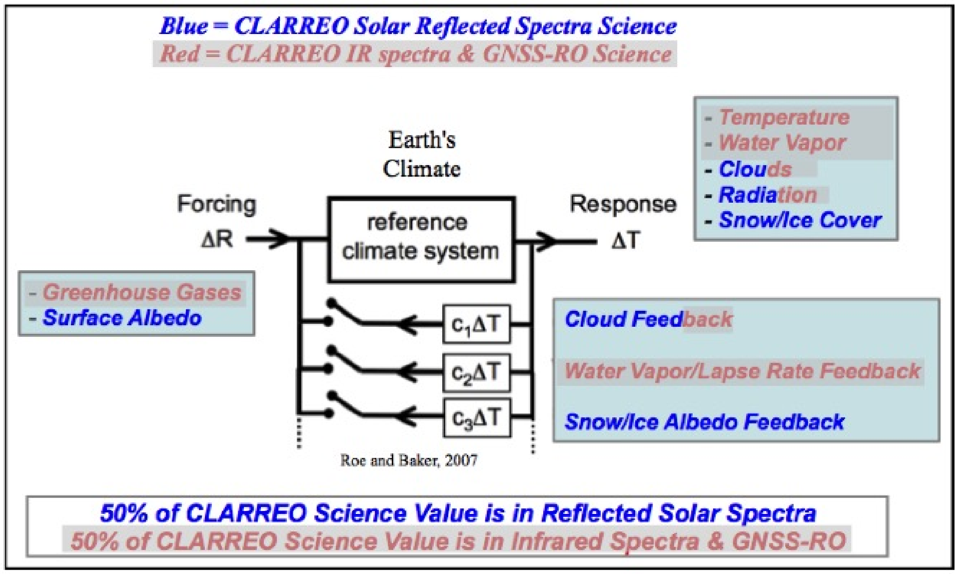

Figure 2.1: The science contributions of the full CLARREO mission, with the parts of that contribution from the RS, IR, and RO specified by color. The IR and RO contributions (red) have been grayed out here to show what will not be contributed to by CLARREO Pathfinder Mission.

probe the Earth's atmosphere. The full mission CLARREO design enables measurement, for the first time, of over 95% of the entire spectrum of Earth's thermal emitted radiation (200 – 2000 cm^{-1} or 5 – 50 μm) and its reflected radiation (320 - 2300 nm). Energy within these spectral ranges drives the radiative forcing of climate change, the climate system's response, and the resulting feedbacks that modify climate sensitivity.

The CLARREO Pathfinder mission, although it differs from the full CLARREO mission in several ways (see Section 3.2), will still provide benefits to climate science (see Sect. 2.4 – 2.6 and Figure 2.1). The CPF will demonstrate the technologies necessary for a RS spectrometer to achieve CLARREO-required accuracy and spectral resolution and the pointing system capabilities necessary to intercalibrate other Earth-observing sensors. Its coverage will span 350 – 2300 nm and its SI-traceable absolute accuracy will be unprecedented compared to operational RS satellite sensors. The spectral coverage and high absolute accuracy of the CPF RS spectrometer will allow it to serve as an in-orbit reference spectrometer to calibrate other concurrently operational satellite instruments with RS spectral bands. CPF will serve as a technology demonstration of a RS metrology lab in orbit, thus illustrating a key component of what the full CLARREO mission would be able to achieve (see Section 3.3 on Science Value of CPF).

The remaining subsections in this section will discuss in greater detail the CLARREO Pathfinder rationale behind the demonstration of climate change-level accuracy (Sect. 2.1), demonstration of its ability to serve as an intercalibration standard in orbit (Sect. 2.2), and its demonstration of the Multi-Instrument Inter-Calibration (MIIC) Framework capability (Sect. 2.3). This section will end with an overview of the near-, mid-, and, long-term impacts of the CLARREO Pathfinder mission.

2.1 Demonstration of Climate Change Accuracy

The full CLARREO mission aims to provide highly accurate and SI-traceable decadal change observations sensitive to the most critical but least understood climate forcings, responses, and feedbacks. The required accuracy is determined by the need to detect projected decadal changes in climate above the background signal of natural variability. The full CLARREO mission measurement requirements have, therefore, been driven by the need to detect these small, but critical, climate change-scale trends, rather than instantaneous instrument noise levels. The CLARREO Pathfinder will demonstrate the capability of the technology and methodology within the RS spectrometer portion of the CLARREO mission to achieve the high absolute accuracy levels needed to achieve these goals.

The CLARREO Pathfinder requirements were derived from the full CLARREO mission requirements. Unlike most missions, CLARREO must consider the impact of its science requirements on multi-decadal time scales. This suggests that requirement metrics must be stated in terms of accuracy of decadal climate trends and in terms of time to detect those trends. The former is more relevant to climate model testing; the latter is more easily discussed in terms of relevance to the timing of societal decision making in a cost/value sense. Having determined the CLARREO mission requirements using the rigorous methodology considered below, the CLARREO Pathfinder mission requirements have been stated such that the CPF would serve to demonstrate that the CLARREO mission calibration and inter-calibration capabilities are achievable. However, the currently expected lifetime of the CLARREO Pathfinder (one year) is less than that of the full CLARREO mission (five years), making it difficult to establish a climate benchmark.

The science community has struggled to make rigorous, quantitative climate monitoring requirements [*Ohring et al.*, 2005]. The science diversity of the CLARREO mission (reflected solar, thermal infrared, and radio occultation), along with recent budget challenges across all of science, demanded the development of a rigorous approach. The result of CLARREO science team deliberations is explained below, with specific focus on determining the accuracy requirement for the CPF's area of technology demonstration: the reflected solar spectrometer.

2.1.1 Determining Accuracy Requirements

Even a perfect observing system would be limited in its ability to measure long-term climate forcing and response [*Leroy et al.*, 2008] due to the noise of the climate system's natural variability (e.g. ENSO, 3 – 5 years). Such natural variability creates a "floor" for required accuracy in climate trends, meaning that climate observations need to have uncertainties smaller than natural variability. The key, therefore, is to quantify the relationship between natural variability and observing system accuracy.

Even though climate trends may not be simply linear, the use of statistical linear trend analysis provides a useful metric to compare the impact of different error sources in a robust framework. Extensive literature exists on climate trend analysis [*Leroy et al.*, 2008, *Von Storch and Zwiers*, 2001, *Weatherhead et al.*, 1998], and the CLARREO team has used this approach to quantify and compare the impact of different sources of uncertainty to determine mission requirements. Although CLARREO/CPF data will not only be used to determine trends, trend analysis provides a critical insight into the mission science requirements and to the utility of the observations for decadal climate change science.

Here, an accuracy uncertainty factor, U_a, for climate trend accuracy is defined as the ratio of trend uncertainty for a real climate observing system to that of a perfect observing system limited only by natural variability. The factor is unitless and can be applied generally to any climate variable. A perfect observing system would have a U_a value of 1.0. Any real observing system will have uncertainties that increase the value of U_a above 1.0. Using the results of *Leroy et al.* [2008] on the relationship between trend uncertainties for perfect and real observing systems, we can determine the accuracy uncertainty factor U_a as follows.

$$U_a = \left(1 + \frac{\sigma_{cal}^2 \tau_{cal} + \sigma_{noise}^2 \tau_{noise} + \sigma_{orbit}^2 \tau_{orbit}}{\sigma_{var}^2 \tau_{var}}\right)^{1/2} \tag{2.1}$$

σ_{var} is the standard deviation of natural variability for the climate variable of interest, τ_{var} is the autocorrelation time scale for natural variability, σ_{cal} is the absolute calibration uncertainty of the instrument, τ_{cal} is the absolute calibration time scale (typically instrument lifetime), and the remaining uncertainties (σ_{noise} and σ_{orbit}) and autocorrelation times (τ_{noise} and τ_{orbit}) are for instrument noise and orbit sampling, respectively. Instrument noise time scale is very short, while orbit-related sampling uncertainty tends to be determined by the climate record time sampling interval, typically monthly, seasonal, or annual. Additional error sources can easily be added to the numerator in Equation 2.1 as appropriate for each climate observation. A complete derivation of Equation 2.1 can be found in Appendix A.

The expression for U_a provides a powerful tool for understanding the trade space of climate monitoring observing system design and cost. The autocorrelation time scale, τ, for each uncertainty source represents the number of independent samples that will exist for any climate record of length Δt. If we consider the case of slow instrument calibration drifts in orbit that cannot be detected, or the case of changing absolute accuracy of instruments with time gaps between their deployments to orbit, the resulting relevant time scale for τ_{cal} is the instrument lifetime, typically about 5 years. Using Equation 2.1, we can see that when compared to orbit sampling time scales for annual mean time series, calibration drifts will in general have much more impact on uncertainty in climate trends, except if the orbit sampling uncertainty is caused by a slow systematic drift in the time of day of the observations, as seen in the NOAA polar orbit data in the 1980s and 1990s. Modern polar orbiters, however, are designed to maintain time of day and eliminate this long time scale.

For the CLARREO mission, the requirement was set for all mission observations (reflected solar, thermal infrared, and radio occultation) to have a value of U_a less than 1.2. In other words, CLARREO is designed to observe climate trends with an accuracy to within 20% of that obtained by a perfect observing system (i.e. limited only by natural variability). This method of setting requirements allows a consistent treatment of climate monitoring requirements across diverse climate variables, each with their own estimates of natural variability. The method also avoids the costs of pursuing perfection that may not add much value to observing climate trends, and provides a quantitative "floor" for climate accuracy. In particular, Equation 2.1 shows that when error sources are a factor of 2 to 3 below the level of natural variability, we have reached the point of greatly diminished returns from any further increase in accuracy.

We can also define an analogous uncertainty factor, U_t, that is the ratio of the time to detect a trend using a real observing system to the time to detect a trend using a perfect observing system [*Leroy et al.*, 2008].

$$U_t = \left(1 + \frac{\sigma_{cal}^2 \tau_{cal} + \sigma_{noise}^2 \tau_{noise} + \sigma_{orbit}^2 \tau_{orbit}}{\sigma_{var}^2 \tau_{var}}\right)^{1/3} \tag{2.2}$$

The only difference between Equations 2.1 and 2.2 is that there is a cubed root on the right side of Equation 2.2, rather than a square root. Since the values of U_a and U_t are always greater than 1, because the creation of a perfect observing system is not possible, Equations 2.1 and 2.2 can be combined and simplified to show that

$$(U_t - 1) \approx \frac{2}{3}(U_a - 1) \tag{2.3}$$

that is, that the degradation of trend accuracy for time to detect trends is only 2/3 of the degradation for accuracy in trends. For example, the CLARREO mission's goal for trend accuracy to be within 20% of a perfect observing system ($U_a = 1.2$), equivalently requires that the time to detect trends is within 13% of a perfect observing system ($U_t = 1.13$). If a perfect observing system could detect a temperature trend with 95% confidence in 20 years, then the CLARREO observing system could detect the same trend with 95% confidence but with 13% more time required: 23 years instead of 20 years.

The framework defined by Equations 2.1 – 2.3 gives a simple but powerful way to understand the value of observing system accuracy both for climate trend accuracy, relevant to tests of climate predictions and for time to detect trends, and relevant for public policy decisions. They also provide a way to compare consistent metrics across a wide range of climate variables and a wide range of uncertainty sources in climate observations.

Here we will show an example applying the accuracy uncertainty factor to determine climate change scale-relevant absolute accuracy requirements by focusing on determining the requirements for the CLARREO reflected solar spectrometer, which will be demonstrated by the CPF.

Uncertainty in climate sensitivity is driven by the uncertainty in cloud feedback, which is driven primarily by low clouds [*Bony et al.*, 2006, *Stocker et al.*, 2013, *Soden et al.*, 2008]. To better understand the RS accuracy requirement to reduce the uncertainty in cloud feedback and therefore climate sensitivity, we focused on the shortwave cloud radiative forcing (SW CRF) (also called SW cloud radiative effect) [*Loeb et al.*, 2007, *Soden et al.*, 2008], which is the difference between all-sky and clear-sky reflected TOA flux. Shortwave (SW) Cloud

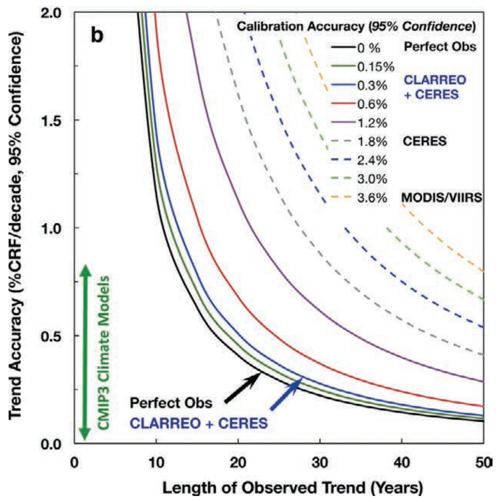

Figure 2.2: This figure shows the relationship between absolute calibration accuracy and the accuracy of decadal cloud forcing trends. The results are shown for a perfect observing system (black curve) and for instruments with varying levels of absolute calibration uncertainty (colored curves). The relationship between RS absolute accuracy and SW CRF trends is shown. This illustrates the dramatic effect of measurement accuracy on both climate trend accuracy (y-axis) and the time to detect trends (x-axis). Accuracy improvements beyond CLARREO approach diminishing returns compared to a perfect observing system.

Radiative Forcing (CRF) natural variability was determined using a 10-year time series of globally and annually averaged CERES data. Additionally, the Student-t distribution was used to account for the short 10-year record of CERES data available. The natural variability estimates determined using CERES data were compared to that of the average of five climate models from the Coupled Model Intercomparison Project phase 3 (CMIP3) (MPI, CanESM2, INMCM4, CCSM4, and GISS) and was found to give a similar estimate to the CERES observations used here. Because instrument calibration uncertainty for reflected solar radiometers is typically quoted in percent reflectance, we considered the relative accuracy of trends in SW CRF in percent per decade.

Instrument noise was set to the CLARREO signal to noise requirement of 30:1 for a solar zenith angle of 75° and a global average albedo of 0.3. CLARREO orbital sampling uncertainties were estimated by simulating CLARREO instrument flights in a 90° polar orbit over the CERES observations used to determine the natural variability. The CERES observations are on a 1° grid; therefore the CERES merged SYN1deg-3hour product was interpolated to hourly time steps and included nadir-only measurements to allow realistic CLARREO-like satellite sub-sampling of Earth's weather and climate fields.

The SW CRF trend accuracy (in %/decade) is shown in Figure 2.2 as a function of the length of the observed trend in years, Δt. The trend accuracies and calibration accuracies in this figure are at a 95% confidence level (k=2). The SW CRF trend accuracies calculated here include uncertainties due to natural variability, absolute calibration (for a range of cases), instrument noise, and orbital sampling (Eqn. 2.1). We show the time to detect trends in SW CRF at various magnitudes for instruments that have a range of absolute calibration uncertainties because it tends to dominate the accuracy of global mean climate variable trends [*Wielicki et al.*, 2013]. The time to detect trends in SW CRF using a perfect observing system is shown by the solid black line and shows the need for long climate records.

A trend magnitude of 1.0%/decade is a level that would be roughly equivalent to a 100% cloud feedback amplification of anthropogenic radiative forcing. Consider that the IPCC-estimated anthropogenic radiative forcing for the next few decades is approximately 0.5 $\mathrm{Wm^{-2}}$/decade [*Loeb et al.*, 2007]. Because the global mean SW CRF is $\sim$50 $\mathrm{Wm^{-2}}$ [*Ramanathan et al.*, 1989], such an equivalent radiative forcing trend would have a magnitude of 0.5/50 = 1.0% per decade in SW CRF. A 50% amplifying cloud feedback would be half as large, or roughly 0.5%/decade. Observing a 50% amplifying cloud feedback in SW CRF would require 22 years of observations at 95% confidence, and observing a 25% feedback would require about 30 years.

The full CLARREO accuracy requirement for the reflected solar spectrometer of 0.3% (k=2) provides an observing system very close in accuracy to a perfect observing system. For the technology demonstration to be provided by the CLARREO Pathfinder, the absolute accuracy requirement is expected to be comparable (see Section 4.1). This accuracy requirement is a factor of 5 to 10 improvement in absolute accuracy compared to operational sensors. The approximate absolute accuracy of operational instruments are shown as dashed lines in Figure 2.2 and include CERES (2%, k=2) and MODIS (4%, k=2). Existing instruments with absolute accuracy levels comparable to instruments like CERES or MODIS must rely upon extensive overlap and assumptions about stability on orbit [*Loeb et al.*, 2007]. Any gaps in these climate records essentially act to restart the climate record because of their reduced absolute accuracy [*Loeb et al.*, 2009].

2.2 Demonstration of Reflected Solar In-orbit Standard

The full CLARREO mission and the CLARREO Pathfinder have both benefitted from the major advances in metrology over the last couple decades [*Brown et al.*, 2006, *Fox et al.*, 2011] and from advances in the techniques to inter-calibrate sensors in orbit. An international effort called the Global Space-Based Inter-Calibration System (GSICS) [*Goldberg*, 2007] arose from the critical need for satellite sensor inter-calibration for research and applications in weather, climate, and natural resources. A major benefit to GSICS activities that is missing from the current observing system, however, are SI-traceable reference radiometers with high absolute accuracy to serve as anchors to the GSICS system. Inter-calibrating two operational instruments, while beneficial, does not include the transfer of SI-traceable absolute accuracy unless at least one of the instruments can serve as such a reference [*Goldberg*, 2007].

Additionally, operational RS instruments (e.g. GOES, MODIS, AVHRR, VIIRS, Landsat) each have different spectral response functions. This challenge implies that accuracy of even relative accuracy inter-calibration is often limited to a few percent since each instrument takes its observation in a different portion of the solar spectrum. A level of uncertainty of a few percent is a factor of 10 larger than what is needed for observing climate change, as discussed in Section 2.1.

A third challenge is sufficiently resolving issues regarding the diversity in polarization sensitivity of RS imagers like MODIS or VIIRS, particularly because this sensitivity varies with instrument scan angle, making the common inter-calibration use of Simultaneous Nadir Overpasses (SNOs) an incomplete calibration approach. The limitations of orbital geometry, when combined with a fixed cross-track scan typical of satellite instruments, limits the ability to match time, space, and angle to nadir view only, making the SNO approach the current state-of-the-art capability for most existing satellite instruments. There are

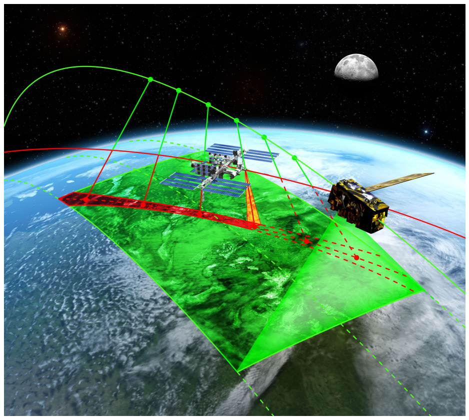

Figure 2.3: As the CPF orbit (ISS; 400 km - red) crosses that of a satellite such as Suomi-NPP (green) with an operational target sensor (e.g CERES, VIIRS), the CPF RS spectrometer collects data matched in time, space, and view angles to provide a reference inter-calibration standard for the target sensors. To match viewing angles with the target instrument, and to maximize the inter-calibration sampling, the CPF RS spectrometer has a 2-dimensional pointing capability with its roll-over azimuth gimbal.

instruments capable of other techniques, however, based upon their design. For example, the CERES instrument, having the ability to rotate the instrument in both azimuthal and elevation direction (i.e. complete a bi-axial scan), has demonstrated that angle, time, and space-matched observations were possible for a wide range of conditions during satellite orbit crossings.

CLARREO Pathfinder will demonstrate both the ability to achieve unprecedented SI-traceable absolute accuracy in orbit and the ability to transfer that calibration to other operational sensors by inter-calibrating with CERES and VIIRS. The CPF will therefore demonstrate its ability, and the ability of a future CLARREO mission, to serve as an SI-traceable calibration reference standard in orbit, providing reference inter-calibration to other instruments to support efforts such as GSICS. Such a demonstration will show how CLARREO will augment the ability of operational satellite instruments to more accurately observe decadal climate change and build long-term climate data records by increasing resilience to data gaps and reducing dependence on assumptions of stability and uninterrupted observation overlap.

A. Inter-calibration Sampling Figure 2.3 shows an example of the CPF on ISS satellite orbit track (400 km altitude and 51.6° orbit inclination) crossing under, for example, the Suomi-NPP or JPSS-1 satellite orbit track (827 km altitude, 13:30LT sun-syncronous orbit with 98.7° orbit inclination). This image also shows the ability to match elevation and azimuth angle across the cross-track scans of CERES or VIIRS. This is accomplished by setting the azimuth angle of the CPF Pathfinder instrument to match the SNPP scan plane and then using the gimbal to slowly rotate the CPF RS spectrometer to match viewing zenith angles across the entire scan during the orbit crossing. The azimuth angle for this match varies for each individual orbit crossing but is essentially constant during any single orbit crossing [*Roithmayr and Speth*, 2012].

The time available for the matching scan is directly proportional to the orbit altitude separation of the two spacecraft. If they are at the same altitude there are only a few seconds available to obtain the entire scan swath, but several minutes are available for an orbit separation of 100 km or more [*Roithmayr and Speth*, 2012]. The orbit of the CPF aboard ISS at an altitude of ∼400 km is well below the typical polar orbiter altitudes of ∼825 km (SNPP, JPSS, METOP), which enables an increase in the matched scan angle inter-calibration time. The orbit of the ISS and the gimbal azimuth and elevation pointing capability will allow CPF to increase reference inter-calibration sampling by more than a factor of 100 compared to current GSICS capabilities, for which typical SNOs restrict polar orbiting satellites to the polar regions and geostationary satellites to the equator.

Reflected solar inter-calibration causes a significant challenge for stringent requirements because of the large spatial and angular variability of reflected solar radiation. A study using AVHRR orbit crossings [*Wielicki et al.*, 2008] showed that space/time/angle matching noise could be reduced to 1% relative for RS inter-calibration if time simultaneity is 5 minutes or less, angle matching in viewing zenith and azimuth angles are within 1° or less, and spatial averaging areas are matched to within 5% of their diameter.

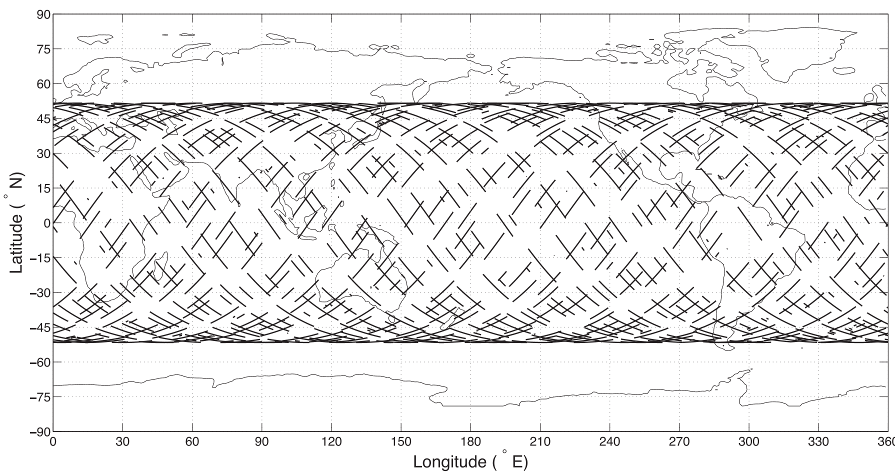

Figure 2.4: Figure 2 from [*Roithmayr et al.*, 2014] shows the locations of inter-calibration opportunities between the ISS and JPSS-1 over a one-year period. The length of each ISS ground track is proportional to the duration of each inter-calibration opportunity.

The ISS is well-suited to serve as a platform from which to obtain RS radiance measurements that can be used to inter-calibrate instruments in sun-synchronous LEO. The ISS orbit provides coverage of a large part of the globe, 51.6°S to 51.6°N latitude. Additionally, scene types necessary for inter-calibration, including clouds, snow, clear-sky ocean, desert, and vegetation, can be found within the area of coverage. Results of orbital simulations show that the difference in ISS and sun-synchronous orbit plane precession leads to temporal uniformity in opportunities for inter-calibration, as shown in Figure 2.4 [*Roithmayr et al.*, 2014]. Angular speed and acceleration required for a two-degree-of-freedom instrument gimbal for matching line of sight on ISS compares favorably to what is required for the CPF on ISS. Our estimates show that the numbers of samples that can be obtained from ISS are sufficient to inter-calibrate well-behaved sensors in sun-synchronous LEO and GEO to the accuracy required for monitoring long-term climate change (Section 2.1).

A unique feature of the CPF RS spectrometer is its on-orbit 2-dimensional pointing ability; this allows for planning and executing inter-calibration operations and maximizing (optimizing) the amount of matched inter-calibration data for a given target sensor. CPF will demonstrate the collection of inter-calibration sampling with CERES and VIIRS on SNPP and JPSS-1. Additionally, the orbital modeling and inter-calibration event prediction developed as a part of CLARREO Science Definition Team activities will serve as a framework for future mission operations.

B. Inter-calibration of Sensor Sensitivity to Polarization Sensitivity to polarization is included in the full CLARREO mission's requirements; however, it has yet to be determined whether polarization will be included in the CLARREO Pathfinder requirements, which is dependent upon whether polarization sensitivity can be accommodated within the CLARREO Pathfinder budget. Because it is still being considered as a possibility for inclusion in the CLARREO Pathfinder mission, in this section, we will discuss the considerations needed for inter-calibrating sensor sensitivity to polarization. Depending on the design of the optics for a spaceborne sensor, its measurements can be sensitive to the polarization of incoming light and have varying response as a function of the polarization state. Typical values of imager sensitivity to polarization are a factor of 2% to 5% depending on the spectral band, increasing for bands in the blue wavelength range [*Sun and Xiong*, 2007]. For the purpose of the CLARREO inter-calibration study reported in [*Lukashin et al.*, 2013], we denote the imager reflectance factor as ρ^{imager}, and consider it without solar zenith factor. We introduce a sensitivity to polarization term to sensor calibration models in a way consistent with the definition by *Sun and Xiong* [2007]:

$$\rho^{imager} = \frac{\rho_0}{(1 + mP)} \tag{2.4}$$

where ρ^{imager} is the derived reflectance including correction sensitivity to polarization, ρ_0 is the reflectance factor corresponding to the imager calibration model for non-polarized light, P is the linear degree of polarization of reflected light at TOA, and m is the sensitivity to the polarization coefficient. The sensitivity to the polarization term is similar to the term for the correction of environment temperature. Both terms correct sensor effective gain. Generally, sensitivity to polarization is a function of sensor scan and polarization angles, $m(\theta, \chi)$. However in our case, Equation 2.4 is defined for fixed sensor scan and polarization angles. The advantage in this approach will be shown below in the clear error propagation analysis. For definitions of the degree of linear polarization, P, and polarization angle, χ, see Appendix B.

Inter-calibration on orbit is achieved by comparing the sensor measurements to observations by CLARREO that are coincident in time, space, and viewing angle, as described above, and considered to be the reference or true observations. Generally, the inter-calibration process is iterative and consists of adjusting the calibration model of the target imager to minimize the differences with the CLARREO instrument. This process would most likely be a joint activity of both the inter-calibrated imager and CLARREO calibration teams. The reference inter-calibration process would start by determining the sensor calibration for the case of unpolarized scattered light (e.g. $P < 0.05$). The second step would be to attribute the differences caused by polarization (e.g. P range from 0.4 to 0.6) to a specific term in the calibration models, such as the inverse term *(1 + mP)* in Equation 2.4. The value of degree of polarization, P, is obtained by applying the Polarization Distribution Models (PDMs) as functions of viewed scene type and geometry. The concept and development of empirical and theoretical PDMs are described in Appendix B.

Because of the physical nature of polarization in an optical system and its linear response, it is reasonable to assume that inter-calibration offsets A_0 or A_p will be very similar, and that the polarization effect will be contained in the difference of inter-calibration gains, G_0 or G_p. Obtaining inter-calibration gain for non-polarized and polarized cases, and attributing the difference to the polarization effect, then imager sensitivity to polarization and its relative uncertainty can be written as

$$m = \frac{(G_p - G_0)}{P} = \frac{\Delta G}{P} \;; \qquad \frac{\sigma_m}{m} = \sqrt{\left(\frac{\sigma_{\Delta g}}{\Delta G}\right)^2 + \left(\frac{\sigma_p}{P}\right)^2}. \tag{2.5}$$

The first term, $\sigma_{\Delta g}/\Delta G$, is random relative error of inter-calibrated gain difference, dependent on inter-calibration sampling. The second term, σ_p/P, is the relative uncertainty of the degree of linear polarization, which we obtain by applying the PDMs (see Appendix B). It is important to emphasize that σ_p is the accuracy of P averaged over a large ensemble of inter-calibration samples, and not the instantaneous error of the PDMs.

After reference inter-calibration of the imager with CLARREO is performed, and the imager calibration model is tuned to minimize its difference with CLARREO measurements, the PDMs are still required to provide polarization information for the imager's stand-alone operations. Sensitivity to polarization and its uncertainty are obtained from inter-calibration results (Equation 2.5). Imager reflectance is expressed by Equation 2.4, where m is the established sensor sensitivity to polarization and ρ_0 is the reflectance obtained from the baseline calibration model adjusted to CLARREO reference. We have demonstrated that the error contribution from polarization angles is small on average. For this study, we assume it to be negligible and that the covariance coefficients for angular parameters are zero. After performing error propagation analysis, we have target sensor relative radiometric uncertainty:

$$\frac{\sigma^{imager}}{\rho^{imager}} = \sqrt{\left(\frac{\sigma_0}{\rho_0}\right)^2 + \frac{P^2\sigma_m^2 + m^2\sigma_p^2}{(1+mP)^2}} \tag{2.6}$$

The uncertainty in the first term, σ_0, is radiometric uncertainty of inter-calibrated VIIRS reflectance for unpolarized measurements. The following steps are required to derive σ_0:

(i) The CLARREO RS-Imager reference inter-calibration data products and the PDMs would be made available to the target sensor calibration team. Data products can range from original Level-1 inter-calibration matched data, matched inter-calibration samples, and CPF team recommendations on effective gain and offset differences, non-linearity, and sensitivity to polarization.

(ii) The target sensor team would use CLARREO reference inter-calibration data and PDMs to improve sensor calibration on orbit. This involves iterative tuning and validation of a complex instrument model to the reference observations and constraints. The goal is to achieve zero bias in the difference between the CLARREO and inter-calibrated sensor reflectances with additional random inter-calibration noise. For an ideal inter-calibration scenario, the uncertainty of the first term in Equation 2.6 can be written as:

$$\frac{\sigma_0}{\rho_0} = \sqrt{\left(\frac{\sigma^{clarreo}}{\rho_0}\right)^2 + \left(\frac{\sigma_{intercal}}{\rho_0}\right)^2 + \left(\frac{\sigma_{residue}}{\rho_0}\right)^2} \tag{2.7}$$

where $\sigma^{clarreo}$ is the accuracy of the CLARREO RS spectrometer, $\sigma_{intercal}$ is the error contribution from inter-calibration noise over an autocorrelation time period, and $\sigma_{residue}$ is error associated with target sensor remaining error contribution (e.g. instrument month-to-month relative stability). These error sources are of different types: bias and random. If the difference between CLARREO and imager measurements has remaining offset/gain, then Equation 2.7 will have additional error terms depending on the quality of performed inter-calibration (remaining inter-calibration offsets and gains).

The second term in Equation 2.6 is the error contribution due to inter-calibrated instrument sensitivity to polarization determined from inter-calibration with CLARREO, uncertainty of sensitivity to polarization, the degree of linear polarization and its uncertainty. When $P > 0$ (and $\sigma_p > 0$), the sensor's radiometric error increases. For a fixed value of sensitivity to polarization, m, it is a function of P, σ_p, and σ_m. The mean m and uncertainty σ_m are obtained from inter-calibration with CLARREO as described above. The degree of polarization and σ_p are obtained from the PDMs.

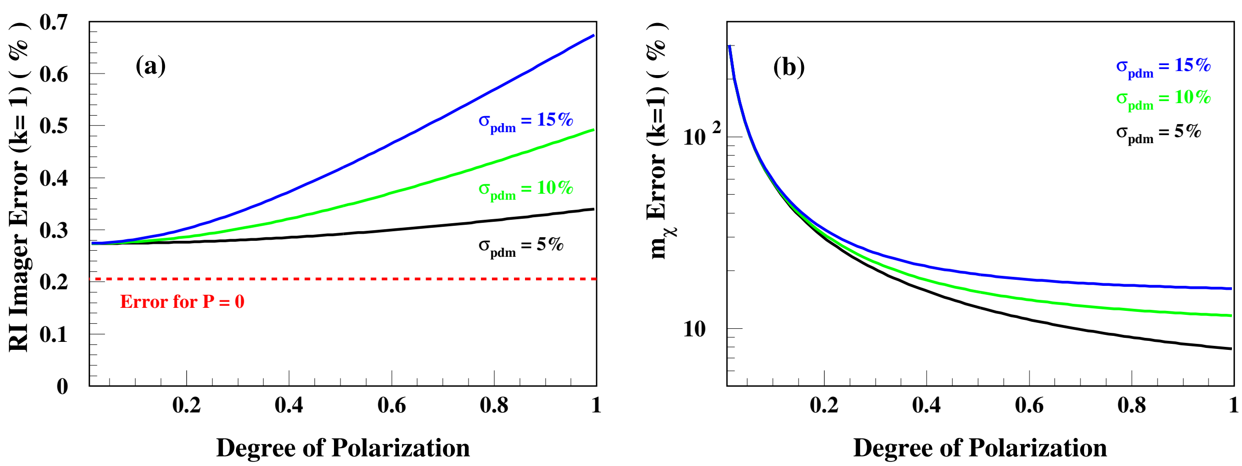

Figure 2.5: (a) Resulting imager relative radiometric error (k = 1) versus degree of polarization. Imager sensitivity to polarization is set to 3% ($k = 1$). Colored curves show cases for different PDM uncertainty, σ_p: 5% (black), 10% (green), and 15% (blue). Red dashed line shows the error level for unpolarized radiances. (b) Estimated relative error of sensitivity to polarization for PDM accuracy of 5% (black), 10% (green), and 15% (blue).

We performed numerical estimates for three different levels of PDM accuracy (σ_p): 5%, 10%, and 15%, using Equations 2.6 and 2.7, and estimated nominal polarized and unpolarized sampling uncertainties [*Lukashin et al.*, 2013]. The resulting imager radiometric uncertainty is shown in Figure 2.5a as a function of degree of polarization. Colored curves show results for PDM accuracy at 5% (black), 10% (green), and 15% (blue). The red dashed line shows the uncertainty level for unpolarized reflectances. In Figure 2.5b, we show results for estimated relative error of inter-calibrated imager sensitivity to polarization and its dependence on the PDM accuracy: 5% (black), 10% (green), and 15% (blue) (Equation 2.5). The estimates show that reduction in PDM accuracy from 5% to 15% can cause an increase in uncertainty of inter-calibrated sensitivity to polarization by a factor of four for fully polarized light.

The CLARREO team has developed a framework for estimation of the resulting uncertainty of CLARREO RS spectrometer reference inter-calibration with an imaging radiometer, such as MODIS, VIIRS, AVHRR, or future imaging instruments on geostationary satellites. To address on-orbit instrument sensitivity to polarization and corresponding radiometric uncertainties, we developed Polarization Distribution Models (PDMs), described in Appendix B.

C. CLARREO RS Instrument Spectral Requirements

The goal of accurate inter-calibration of imaging multi-spectral instruments impacts spectral requirements for the CLARREO Pathfinder reflected solar instrument. We have determined sensitivity of inter-calibration uncertainty on key design parameters of the CPF spectrometer: its spectral range and sampling [*Wu et al.*, 2015].

RS Instrument Spectral Coverage:

One of the objectives of the CPF mission is the calibration of broadband radiance for CERES. For this endeavor, the required spectral coverage is a critical parameter for the CPF RS spectrometer instrument design. Although solar radiation spans a wide spectral range, over 99.5% of the total reflected energy from the Earth to space is within the spectral range from 300 nm to 2500 nm under virtually all real atmosphere-surface conditions, as shown in Figure 2.6a for selected surfaces and Figure 2.6b for all-sky averages. Therefore, in terms of total radiation, measurements do not need to cover the entire spectrum but only the range in which sufficient reflected solar energy is enclosed. The minor correction from the uncovered spectral regions can be made using radiative transfer calculations.

Summary of estimated error in total reflected solar energy is shown in Table 2.1 as a function of instrument spectral coverage globally and for selected scene types.

Scene Type	320 – 2300 nm	320 – 2400 nm	310 – 2300 nm	310 – 2400 nm
Global	0.09%	0.07%	0.05%	0.03%
All-sky Ocean	0.10%	0.08%	0.04%	0.03%
All-sky Land	0.08%	0.06%	0.05%	0.04%
Clear Ocean	0.16%	0.15%	0.05%	0.04%
Clear Desert	0.10%	0.07%	0.07%	0.04%

Table 2.1: Estimated error in the total reflected solar energy.

RS Instrument Spectral Sampling and Resolution:

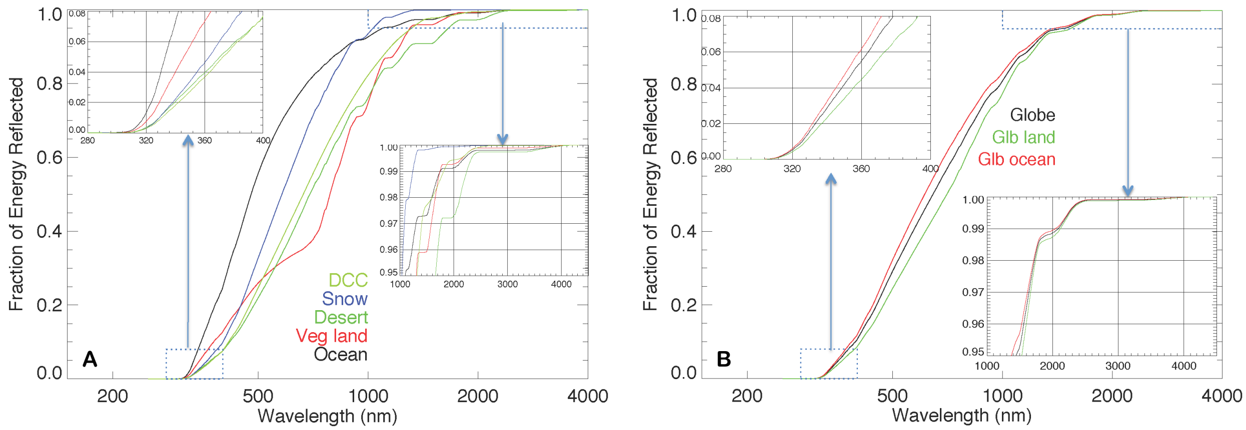

Figure 2.6: (a) The cumulative distribution of the Earth's reflected solar energy at the nadir view of ocean, vegetation land, desert, and snow surfaces under clear skies and for the deep convective cloud with optical depth of 200. The y-axis shows the cumulative fraction of the reflected solar radiation. The standard mid-latitude atmosphere is used in the calculations with solar zenith angle as 45°. (b) The cumulative energy distribution of the monthly global, ocean, and land mean radiation. The calculations used the observational data for aerosol, cloud, and surface properties from MODIS/CERES.

Signal aliasing arises when a signal is discretely sampled at a rate that is insufficient to capture the changes in the signal. In the case of inter-calibration, spectral reflectance aliasing will result in additional systematic uncertainty, which can be avoided with a proper sampling rate. The Nyquist-Shannon sampling theorem provides a prescription for the nominal sampling interval required to avoid aliasing. Molecular absorption in the oxygen A-band (760 nm) contains features that change with wavelengths faster than 0.1 nm. In comparison, the water absorption features include changes within wavelength intervals of 1 – 2 nm. The Earth's reflectance spectra, outside of molecular absorption, are relatively smooth, and these spectral regions are the high priority for the CPF inter-calibration objectives.

To estimate the expected biases due to CLARREO (and therefore CPF) RS spectral sampling, we used theoretical calculations (MODTRAN) and the SCIAMACHY Level-1B data product (SCI_NL_1P) to obtain nadir spectral reflectance with wavelengths ranging from 240 nm to 1750 nm [*Bovensmann et al.*, 1999]. The impact of spectral resolution is tested using a number of reduced sampling frequencies from 1.0 to 8.0 nm. To produce each of the reduced sampling data sets, an integral of a Gaussian distribution (i.e., normal distribution) function with bandwidths being two times the sampling frequency (the Nyquist rate) is applied to the original high resolution spectral data. The MODIS band reflectances are computed by using relative spectral response functions.

In Figure 2.7a, we show the spectral sampling with 4 nm frequency and 8 nm Gaussian Full-Width at Half-Maximum (FWHM) bandpass (black), the baseline requirement for the CPF RS instrument, and re-sampled all MODIS reflective solar bands (solid circle). The results are based on all-sky SCIAMACHY instantaneous data from July 2004, providing a general picture of how representative a CLARREO RS-like instrument would be in the inter-calibration of MODIS reflective solar bands. Figures 2.7b and 2.7c show expected reflectance aliasing at the same six MODIS bands for SCIAMACHY nadir sampling of deep convective

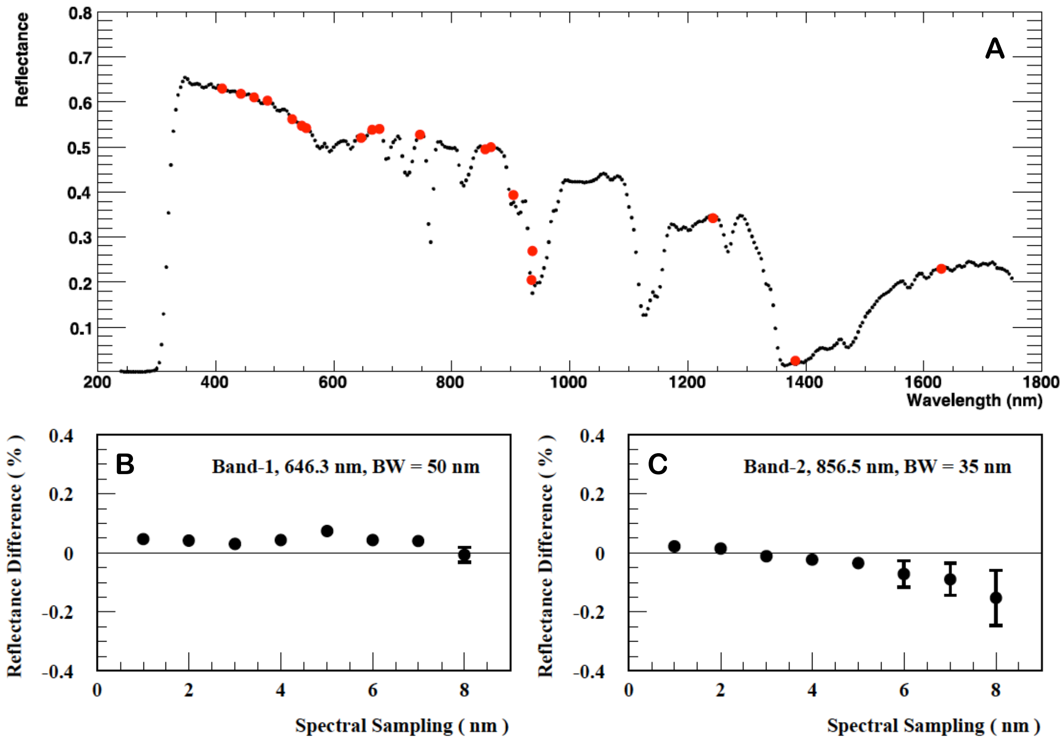

Figure 2.7: (a) Spectral sampling with 4 nm frequency and 8 nm Gaussian Full-Width at Half-Maximum (FWHM) bandpass (black), recommended for CLARREO RS Spectrometer, and re-sampled MODIS bands (red circle). The results are based on all-sky SCIAMACHY instantaneous data from July 2004. (b) and (c) Expected reflectance aliasing at two MODIS bands as a function of spectral sampling frequency. Deep Convective Clouds in July 2004 SCIAMACHY instantaneous data. The error bars show standard deviation of the difference (k=1).

clouds with solar zenith angle (SZA) $< 70°$, and latitude within 60° North to 60° South. In this Figure, relative difference in spectral reflectance between calculated MODIS band reflectance from original high-resolution and re-sampled spectra is plotted as a function of sampling frequency. For the CPF baseline 4 nm spectral sampling requirement, the estimated biases are below 0.1% for wavelength outside absorption.

Results of our studies indicate that the current concept of the CPF RS instrument with a spectral range from 350 to 2300 nm, a 4 nm sampling resolution and 8 nm resolution (FWHM) will satisfy the inter-calibration standard requirements. Errors in total reflected energy can be corrected, and estimated spectral biases are below 0.1% for wavelengths outside absorption regions. For the water vapor absorption bands, the challenge remains due to sensitivity to the spectral features of atmospheric water vapor absorption.

2.3 Demonstration of Multi-Instrument Inter-calibration Framework

Climate quality measurements require accurate calibration. Inter-calibration ties the calibration of one instrument to a more accurate, preferably SI-traceable, reference instrument by matching measurements in time, space, wavelength, and view angles. The challenge is finding and acquiring these matched samples from within the large data volumes distributed across international data centers. For inter-calibration, typically $< 0.1\%$ of the data volume is required for analysis. Software tools and networking middleware are needed to intelligently select and acquire matched samples from multiple instruments on separate spacecraft. Matched instantaneous observations are also used in cloud, aerosol, and model comparative analysis studies.

The Multi-Instrument Inter-calibration (MIIC) Framework is a collection of software to support inter-calibration and inter-comparison studies within NASA and NOAA data systems. Its collection of software works in a distributed collaborative environment to support LEO-GEO and LEO-LEO inter-calibration and inter-comparison studies. Development of the MIIC framework started with SMD ROSES ACCESS 2011 funding. The project continued to be funded by the SMD ROSES ACCESS 2013 program. Currently, the effort is focused on extending MIIC data access and analysis features and deploying MIIC web services.

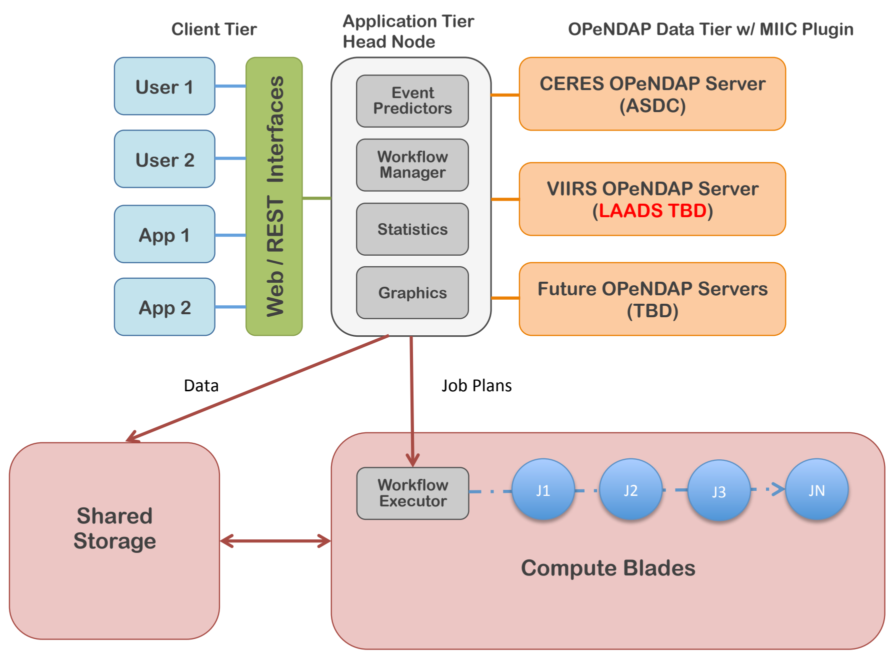

Figure 2.8: The MIIC framework multi-tier configuration for CLARREO Pathfinder: client, application, and OPeNDAP data tiers.

Inter-calibration between instruments is a central pillar of the calibration-validation strategies of many national and international satellite remote sensing organizations. GSICS, an international collaboration focused on inter-calibration of space-borne sensors, recommends a variety of algorithms. Most are based on matching data from Earth targets or simultaneous nadir overpasses. All organizations comparing observations from multiple instruments face the same challenge – how to access matched measurements from within large datasets distributed across multi-agency international data centers. The typical process is to spend months of time downloading data from remote data centers onto Terabytes (TBs) of expensive disk space. Custom non-reusable software is written to read and process data on local client machines. Results are published, but code is typically poorly developed, maintained, and results hard to duplicate. Alternatively, common reusable software helps to alleviate some of these problems.

The MIIC framework multi-tiered architecture that is planned to support the CLARREO Pathfinder is shown in Figure 2.8. The MIIC framework provides three main web services: Event Prediction, Data Acquisition, and Analysis.

The Event Prediction service finds collocated near-coincident measurements with similar view conditions based on viewing zenith, solar zenith, and relative azimuth angle differences. The framework uses an open source orbit propagator (SGP4) and custom Earth rotation, solar position, and instrument scan models to predict matched observations. This service is fast and efficient since no data products are read; instead, only daily two-line-element (TLE) files are processed. The Event Predictor outputs Latitude-Longitude bounding boxes with instrument scan start/stop times for each matched event within the specified time period. Time periods can be days, months, or years so long as satellite TLEs exist. An example of inter-calibration event prediction is shown in Figure 2.9 for daytime measurements from MODIS and GOES-13 for January 1, 2011.

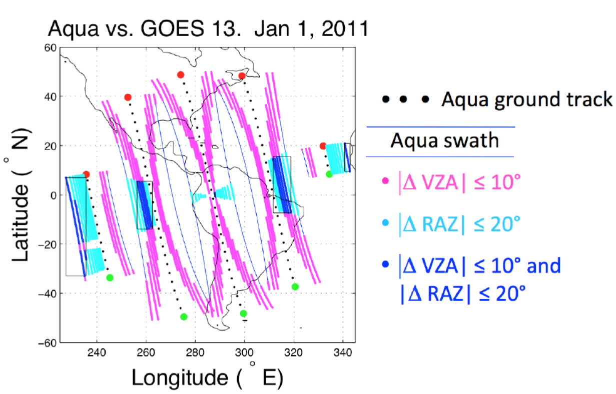

Figure 2.9: LEO-GEO Event Prediction for daytime measurements from MODIS and GOES-13 on January 1, 2011.

The Data Acquisition service then parses the Event Acquisition plan and communicates over the network using the OPeNDAP network protocol to acquire events from each remote data center. OPeNDAP server-side grid averaging, spectral and spatial convolution, and histogram functions are executed on remote servers. This combination of event prediction and server-side functions eliminates the need to transfer large volumes of data files in entirety, reducing both data center and user network bandwidth and disk storage consumption. Users can more efficiently access NASA data through the RESTfull Application Programming Interfaces instead of point-and-click file selection order tools. The LEO-GEO MODIS/GOES-13 inter-calibration use case shown in Figure 2.9 demonstrates a significant reduction in data transmission. One month, January 2011, of Aqua/MODIS L1B and GOES-13 imager data consists of 9672 files (1.4 TB). The Event Prediction algorithm, which finds time-matched simultaneous overpasses, reduces the number of files transmitted by a factor of 22. Server-side equal angle spatial grid averaging reduces the data by an additional factor of 34. The final matched gridded MODIS/GOES-13 samples are contained in 808 files (1.8 GB). This is consistent with other LEO/GEO inter-calibration algorithms that typically require only 0.1% of the total data volume.

In addition to the substantial reductions in data transfer, there is a more important qualitative benefit provided by services such as the MIIC Framework. New collaborative research becomes more feasible as critical data centers such as NASA's Atmospheric Science Data Center support value-added services along with remote access to their data.

Costs to transfer and store large volumes of data sets for inter-comparison studies are significant, especially when years of data and reprocessing are considered. Instead, acquiring only matched samples and performing more calculations at the data source enables better utilization of existing resources. Powerful event prediction and server-side processing simplifies data accessibility and enables researchers to focus more on analysis tasks. The MIIC Framework is based on demonstrated technology levels greater than TRL 6.

2.4 Near-term Earth Science Impacts: 1 year

Despite the relatively short planned lifetime of the CLARREO Pathfinder (one year), there are many near-term impacts that help advance and reduce risk for the full CLARREO mission within this time frame, such as:

- Providing a year of on-orbit crossing data with Suomi-NPP, JPSS-1, MetOP, Terra, Aqua, and geostationary satellites (5 for global coverage). With additional project funding, all of these data may be able to be used to demonstrate the inter-calibration capability; however, the Pathfinder's technology demonstration only includes inter-calibration demonstration with CERES and VIIRS;
- Demonstrating the use of the RS spectrometer as a reference instrument for inter-calibration as part of GSICS (Global Space Based Inter-Calibration System);
- Putting the lunar spectral irradiance on an SI-traceable scale with 10 to 20 times the current accuracy of 5 to 10% (k=1);
- Potentially characterizing a sample of surface sites such as Dome-C and the Libyan desert for Landsat inter-calibration and demonstrating the capability of an accurate surface Bidirectional Distributions Reflectance Function (BRDF) spectral product for the full CLARREO mission. A new BRDF product would serve as a benefit to climate modeling and climate OSSE communities.

2.5 Mid-term Earth Science Impacts: 2–3 years

Assuming the RS instrument is preforming well on orbit (i.e. achieving climate change accuracy, acceptable instrument noise, and acceptable duty cycle) and that the mission is extended beyond the initial year, there are several mid-term impacts and benefits that can be expected from CPF. During a potential 2nd and 3rd year of the CPF technology demonstration, the following could be accomplished if funded as extensions:

- Quantify interannual variability of the reflected solar spectra
- Use of the RS calibration reference instruments through monthly inter-calibration over 3 years to detect trends in calibration change of operational instruments with RS bands such as VIIRS, AVHRR, CERES, and geostationary satellite imagers.

2.6 Longer-term Earth Science Impacts: 4–5 years

Assuming that the RS instrument is preforming well on orbit and the mission is extended beyond a potential 3rd year, there are numerous benefits that could be realized. During a potential 4th and 5th year of the technology demonstration, the following could be accomplished:

- Provide an initial anchor for a climate record benchmark at levels of accuracy a factor of 5 to 10 beyond existing instruments.
- Extend the statistical reliability of the interannual natural variability for RS spectral fingerprints of climate change examined in the 2nd and 3rd years by covering a full normal 5 year ENSO cycle (i.e. one including both El Niño and La Niña phases).
- Extend the ability to determine long-term calibration drifts in a wide range of Earth observing sensors in LEO and GEO.
- Extend the lunar irradiance spectral calibration to include more lunar cycles and thereby verify the variations due to libration of the moon.
- Verify the calibration capability of the RS instrument over the full 5 year nominal instrument lifetime of future CLARREO missions.
- Incorporate any lessons learned into future instrument designs for a full CLARREO mission, further reducing risk.

3 CLARREO Pathfinder Mission on ISS

3.1 CLARREO Pathfinder Mission Concept

CLARREO Pathfinder will fly the CLARREO reflected solar (RS) instrument on the International Space Station (ISS). Due to the ISS inclination orbit of approximately 51.6°, CPF will not have coverage of Earth's polar regions; however, flying in a precessing orbit will significantly enhance sampling for inter-calibration of existing sensors, which is one of the primary objectives of the CLARREO Pathfinder. The CLARREO Pathfinder mission architecture comprises three major areas: the Space Segment, Ground Segment, and Science Segment.

The CLARREO Pathfinder Space Segment consists of an ISS external payload, constrained by the trajectory and attitude of the ISS, and it relies on the ISS to provide electrical power and a communications link to the CLARREO Pathfinder Ground Segment. The RS instrument will reside on the Expedite the Processing of Experiments to the Space Station (ExPRESS) Logistics Carrier-1 (ELC-1), a vertical structure extending in the nadir direction from the port wing of the ISS. CLARREO Pathfinder systems engineers are currently comparing the performance characteristics to optimize the calibration and inter-calibration capabilities of the CPF instrument between two payload attachment points on ELC-1: 1) Site 3 on the outboard side of ELC-1, providing views in the ram, port, and nadir directions; and 2) Site 8 on the inboard side of ELC-1, providing wake, starboard, and nadir views.

The primary technical performance measures that the team is evaluating involve lunar and solar calibration and inter-calibration opportunities. Each ELC-1 site being considered provides different distributions of lunar calibration opportunities, varying in the number, temporal distribution, and lunar phase angle distribution. Similar challenges are presented for solar calibration, excluding the phase angle distribution challenge. Additionally, the team is evaluating which site optimizes inter-calibration opportunities to ensure mission success.

The CLARREO Pathfinder Ground Segment links the data flowing between the ISS and Science Segment, and its primary functions are performing Level 0 processing of downlinked science telemetry (TLM) data and queuing payload commands for subsequent uplink to the Space Segment. From the perspective of CLARREO Pathfinder, the ISS Program infrastructure acts as a bent-pipe repeater of Space Segment-generated science TLM data. While the ISS Program adds various data wrappers to the science TLM data during transit among multiple facilities, those data flow out of the ISS Program ground infrastructure in the same format in which they enter the ISS vehicle's data systems on orbit.

The CLARREO Pathfinder Science Segment transforms the Level 0 science data processed by the Ground Segment into Level 1 and Level 4 science data products (see Section 4.1.2). The Science Segment also manages the storage and distribution of CLARREO Pathfinder science data, the inter-calibration of CLARREO Pathfinder science data with those of other Earth-observing systems, and the science-related tasking of the CLARREO Pathfinder payload on-orbit.

3.2 Differences Between CLARREO Pathfinder and full CLARREO

The benefits of CLARREO Pathfinder and its contribution to the future success of the full CLARREO Mission are numerous. There are, however, several limitations of CLARREO Pathfinder when compared to the full CLARREO mission. Explicit differences between CLARREO Pathfinder and the full CLARREO mission concept as of its Mission Concept Review in 2010 are as follows:

- A low-cost pathfinder on ISS should not be expected to achieve the full complement of scientific goals of a full CLARREO mission (conducted on one or more specialized free-flyer spacecraft); however, it can be expected to achieve the risk-reduction goals mentioned prior and to demonstrate the full performance of the calibration and verification systems for the reflected solar portion of the full CLARREO mission.

- The short planned lifetime (one year) of the CLARREO Pathfinder will likely result in a record shorter than the 5 years of observations needed to begin the CLARREO full mission spectral fingerprint benchmarks (L2 and L3 data products).
- The CLARREO Pathfinder budget will support full Level 0 processing but will not support complete Level 2 and 3 processing. No level 2 or 3 processing is planned. Level 4 processing is limited to that sufficient to demonstrate inter-calibration for the Clouds and the Earth's Radiant Energy System (CERES) and Visible Infrared Imaging Radiometer Suite (VIIRS).
- If CPF is judged to be highly successful, meaning that the team has advanced the technology development and delivered useful science, NASA HQ may decide at a later time to fund processing of the Pathfinder Level 0 observations to provide full CLARREO mission L1 through L4 data products.
- GNSS-RO observations are not obtained on ISS and the IR spectrometer has not been defined to be a part of the CLARREO Pathfinder.

Figure 3.1 shows the key differences between the full CLARREO Mission and CLARREO Pathfinder; however, note that the specific requirements for CLARREO Pathfinder are still in development. The requirements listed in Figure 3.1 are representative of what the requirements for CLARREO Pathfinder are likely to be and are included to present an illustration of the differences between the full CLARREO Mission and the CLARREO Pathfinder Mission.

Parameter	Full CLARREO	CLARREO Pathfinder
Science Objectives	• Document changes in the climate system • Make highly accurate and SI-traceable decadal change observations • Improve calibration traceability for EOS assets	• Demonstrate essential measurement technologies of the CLARREO Tier 1 Decadal Survey mission • Demonstrate on orbit, high accuracy, SI-Traceable calibration • Demonstrate ability to transfer to other in-orbit assets
Mission Lifetime	5+ years	1-2 years (Baseline: 1 Year; Threshold: 8 months)
Mission Class	Class C	Class D
Orbit	P90	ISS 52º Inclination
Data products	L1 -- L4 (GNSS-RO: L2; Benchmark: L3)	L1 (L4 for CERES, VIIRS, & CrIS)
Reflected Solar	2 instruments	1 instrument
Accuracy	Absolute uncertainty ≤ 0.3% (k=2)	Baseline: • Broadband: < 0.5% (k=2) • Spectral < 1% (k = 2) • 0.3% (k=2) at 700 nm - 1000 nm, and 1% (k=2) at 350 - 2300 nm Threshold: • Broadband: <1% (k=2) • Spectral: < 2% (k=2) • 1% (k=2) at 700 nm – 1000 nm, and 3% (k=2) at 350 – 2300 nm
Spectral Range	320 nm to 2300 nm	350 nm to 2300 nm (baseline and threshold)
Resolution	4nm sampling and 8 nm bandwidth	Baseline: 4 nm sampling and 8 nm bandwidth Threshold: 8 nm sampling and 16 nm bandwidth
Infrared	2 instruments	None
Accuracy	Systematic error ≤ 0.1 K radiance calibration uncertainty (k=3)	N/A
Spectral Range	200-2000 cm^{-1}	N/A
Resolution	0.5 cm^{-1} unapodized	N/A
GNSS-RO	2 instruments	None
Reference Inter-calibration	• Broadband CERES • Operational sounders (e.g. CrIS, IASI) & imagers (e.g. VIIRS, AVHRR, Landsat) • Geo assets (all) • Vicarious calibration targets	• Broadband: CERES • Operational Imager: VIIRS • GEO and land imagers (data collection, no analysis) • Vicarious calibration targets (limited)

Figure 3.1: Table comparing the mission differences between the full CLARREO Mission and CLARREO Pathfinder on ISS. For more information about the full CLARREO Mission, please see the CLARREO Science Definition Team Report.

3.3 CLARREO Pathfinder Science Value Matrix

The CLARREO science value matrix (SVM) is a concept that has been used to clarify and quantify, for both NASA Headquarters and the CLARREO team, the value of various mission trade studies during pre-phase A work. Additionally, it has also helped to quantify the value of various mission options for the CLARREO Pathfinder Mission. It has assisted the team in clarifying its thoughts on the wide range of climate science that might be impacted by CLARREO and CLARREO Pathfinder observations. The CLARREO mission concept is unusually broad in this regard: most NASA missions focus on measuring one or two climate variables, and therefore, a SVM is of less use. CLARREO's breadth of science impact is a unique strength, but it can also complicate derivation of the mission priorities and requirements. The science value matrix is one of the tools used to help with this challenge, assisting the team in converging on and justifying its decisions and recommendations.

For a SVM to be a useful tool, the "value" needs some method of quantification. The science value matrix approach is based on the CLARREO team's work and discussions in Section 2. The Science Value of a Science Objective, SV_{so}, is computed using the following product:

$$SV_{so} = F_{si} \times F_{cov} \times F_{cv} \times \sqrt{F_{crl}} \times F_{ta} \times F_r \quad (3.1)$$

F_{si} is the science impact factor, F_{cov} is the global coverage factor, F_{cv} is the calibration verification factor, F_{crl} is the climate record length factor, F_{ta} is the trend accuracy factor, and F_r is the risk factor. If any objective has zero science impact, there is no value in measuring it, no matter how accurately it is measured or how low-risk the measurement can be done. If the climate record length is too short, the data has little utility and is lost in natural variability. If the accuracy is too poor, CLARREO and CPF would add little value over existing sensors. As a result, the overall science value is dependent on the multiplicative (not additive) total of the above factors. In this section, the definition of each factor in Eqn. 3.1 is briefly discussed. Note that in all cases the factors used in this equation are relative measures of value. In general, the CLARREO MCR Baseline Mission is assigned "100% Science Value" (more about the CLARREO MCR Baseline Mission can be found in the CLARREO SDT Report), and the value of CLARREO Pathfinder mission options will be scaled to the Baseline Mission science value. In the text below, the Science Value of the CLARREO Pathfinder mission (only the RS) and the other CPF mission options (only the IR and RS+IR) for direct comparison of their science values relative to the CLARREO MCR Baseline mission, will be discussed.

Science Impact Factor

The science impact factor, F_{si}, serves to capture both the importance of the science objective as well as the uniqueness of the CLARREO contribution to it. Each science contribution is assigned a relative numeric weight, and these values are common to all possible mission scenarios. Climate forcing, response, and feedback science objectives have equal values. This fits well with IPCC discussions of decadal to century climate change, as well as the diagram summarizing CLARREO science objectives, shown in Figure 2.1.

The science impact factors, third column from the left in Table 3.1, are based on the IPCC uncertainties in forcing, response, and feedback components [*Stocker et al.*, 2013]. Cloud feedback uncertainty is roughly twice as large as water vapor and lapse rate feedback uncertainty [*Bony et al.*, 2006, *Stocker et al.*, 2013, *Roe and Baker*, 2007, *Soden and Held*, 2006]. Cloud feedback uncertainty is roughly three times larger than the snow/ice albedo feedback uncertainty [*Bony et al.*, 2006, *Stocker et al.*, 2013, *Roe and Baker*, 2007, *Soden and Held*, 2006]. This results in a total science impact weight of 4 to cloud feedback, 2 to

CLARREO Pathfinder on ISS: 1 RS (2020).							
CLARREO Science Objective	**Related Climate Change Variable**	F_{si}	F_{cov}	F_{cv}	$\sqrt{F_{crl}}$ (70%)	F_{ta} RS	SV_{so}
Cloud Feedback SW	Reflected SW flux, albedo RS Cloud Properties	**2**	0.83	1.5	1.4	1.0	**3.5**
Cloud Feedback LW	Earth Emitted LW flux IR Cloud Properties	**1**	0.83	0	0	0	**0**
Cloud Feedback Net	Net Cloud Radiative Forcing	**5**	0.83	0	0	0	**0**
Temperature Response & Lapse Rate Feedback	Temperature Profile	**3**	0.83	0	0	0	**0**
Water Vapor Response & Water Vapor Feedback	Water Vapor Profile	**3**	0.83	0	0	0	**0**
Aerosol Direct Radiative Forcing	Aerosol Radiative Forcing Aerosol Properties	**1.5**	0.83	1.5	1.4	1.0	**2.6**
Snow & Ice Albedo Feedback	Reflected SW flux, albedo Snow/Ice & Cloud Cover	**1.5**	0.83	1.5	1.4	1.1	**2.7**
Land Albedo Change & Radiative Forcing	Reflected SW flux, albedo	**0.5**	0.83	2.0	1.4	1.1	**1.2**
Vegetation Index Change	Vegetation Index	1	0.83	2.0	1.4	1.1	**2.4**
Sum of Mission Science Value							**12.5**
Total Mission Science Value relative to MCR Baseline							**16%**

Table 3.1: Science Value Matrix for the CLARREO Pathfinder Mission, which includes the CLARREO reflected solar spectrometer only. The only factor not shown here is the risk factor, which, as discussed, is estimated to be approximately 1.0 for all CLARREO/CPF mission options. The total science value of the CLARREO MCR Baseline Mission is used as a reference.

water vapor/lapse rate feedback, and 1.5 to snow/ice albedo feedback. Consistent with the earlier discussion of giving equal value to feedback and response, a science impact value of 4 is added to climate change responses relative to cloud feedback (flux, cloud properties), so that the total impact value is 8. Given the importance of the temperature and water vapor profile response in the NRC decadal survey [*National Research Council*, 2007], a total value of 4 is assigned to the temperature/water vapor response. The resulting cloud feedback/response impact totals 8 (4 feedback + 4 response), and the resulting temperature water/vapor impact totals 6 (2 feedback + 4 response).

Since the full CLARREO mission's information content varies quite a bit among the RS, IR, and RO observations, the science impact is further divided among the individual observational components. This allows the CLARREO mission to consider the relative impact of different components of its observations. Cloud feedback is separated into its LW, SW, and net components. Climate sensitivity is linked most directly to net cloud feedback, which is the combination of SW and LW cloud feedbacks [*Soden et al.*, 2008]. Of the total impact of 8 for cloud feedback, 5 of those units are assigned to net cloud feedback. The remaining science impact is 2 for SW and 1 for LW cloud feedback. The larger impact score for SW is based on the largest IPCC uncertainty in cloud feedback having been identified as low cloud feedback [*Bony et al.*, 2006, *Stocker et al.*, 2013]. Low clouds are dominated by the SW cloud radiative effect and have a much smaller influence on LW cloud radiative effect. Therefore, an impact of 2 is assigned to the SW cloud feedback, and 1 to the LW cloud feedback. SW impact is assigned to the RS spectrometer and LW impact would be relevant for an IR spectrometer. Net impact requires measurements from both RS and IR spectrometers.

The six units of science impact equality for temperature and water vapor are divided equally, with 3 assigned to temperature lapse rate feedback and response and 3 to water vapor feedback and response. For water vapor, the science impact is relevant to measurements made by the IR spectrometer, while for temperature, it would be split between the IR spectrometer and the RO instrument.

For radiative forcing, a factor of 4 is given to the uncertainty in aerosol direct and indirect radiative forcing. However, CLARREO and CPF are assumed to contribute only an impact of 1.5 out of the full aerosol uncertainty. The radiative forcing uncertainty due to land albedo change is much smaller than that of aerosols and the factor of 0.5 science impact reflects this reduction [*Stocker et al.*, 2013]. Finally, vegetation index change as a measure of biosphere changes is also given a relatively low weight of 1. At this time, it is more difficult to quantify this weight than the others.

Global Coverage Factor

The global coverage factor, F_{cov}, is defined to represent the scope of reference intercalibration and spectral fingerprinting capability that could be achieved by the mission option. Although the mission success of the CLARREO Pathfinder mission is not dependent upon its ability to conduct benchmarking and spectral fingerprinting, the RS instrument will be capable of taking measurements that could be used to start a climate benchmark and to conduct spectral fingerprinting. If the funding becomes available, the spectral fingerprinting capability and software will have the opportunity to be developed. For the full CLARREO mission, 50% of its mission value is for reference intercalibration, and the other 50% is for climate benchmarking. Being in the orbit of the ISS allows the CLARREO Pathfinder to achieve the full intercalibration capability. However, measurements of the polar regions (poleward of 51.6°) cannot be made in the ISS orbit. For climate benchmarking, about one-third of its value can be assigned each to the tropics, the mid-latitudes, and the polar regions. Therefore, with the CPF being constrained by the orbit of the ISS, it achieves 0.67 of the full global climate benchmarking capability. By weighting this value with the full intercalibration part of the mission, the global coverage factor obtained is 0.83. Although for simplicity the F_{cov} values are not shown here, they are the same for all science objectives for both alternative CPF options of IR only and RS+IR.

Calibration Verification Factor

The CLARREO mission SVM defines this factor, F_{cv}, as follows: a value of 2 is given to independent verification of the CLARREO/CPF observation, and a value of 1 is given to a CLARREO/CPF observation without independent verification. Clearly there can be an open and lengthy discussion about the independent verification that will serve this purpose for each observation. As for the science impact value, this metric will not be as simple as the trend accuracy or length of climate record metrics. Nevertheless, given the CLARREO task of high confidence in decadal change, it seems inescapable that CLARREO include such a metric.

Current values of this metric are very rough. A verification factor of 2 is assigned to a science objective if there is a 1-year overlap of two CLARREO instruments in-orbit to verify consistent performance and calibration within uncertainty of the instrument or instruments used for that science objective. If there is no overlap, then the verification factor depends on an evaluation of the independent ground calibration of RS spectrometers by different organizations. If a partial verification is possible, it is given a factor of 1.5 in the current tables. The likelihood of achieving in-orbit instrument overlap is taken into account by using the probability of obtaining overlap as a weighting function; however, overlap is not currently included in the plan for the CLARREO Pathfinder.

For example, for a 2017 and 2020 launch of a single IR spectrometer on each spacecraft, there is a 70% probability of 1 year of overlapping data. If the verification factor for no in-orbit overlap is 1.5 (aircraft verification), while having overlap is 2.0, then the probability of overlap in orbit is used to obtain a verification factor weighted between the 1.5 and 2.0 values, in this case $1.5 + (0.7) \times (2.0 - 1.5) = 1.85$. This is a very simple and crude method that allows some accounting for the relative value of instrument overlap in-orbit, as well as the likelihood of obtaining it based on launch schedules and instrument and spacecraft reliability.

Trend Accuracy Factor

Here, trend accuracy means the relative accuracy for CLARREO determination of decadal change trends. This metric is determined by the accuracy relative to a perfect climate observing system limited only by natural variability [*Leroy et al.*, 2008]. The metric quantifies the effect of instrument absolute accuracy on the uncertainty of trend detection, as well as the effect on time to detect climate change trends at a given level of confidence. Climate trend accuracy is key to testing climate model predictions of decadal change, while time to detect trends is key to societal decision making processes. The extension of the *Leroy et al.* [2008] results include all CLARREO sources of uncertainty, such as instrument noise and orbital sampling (see Section 2.1).

Equations 2.1 – 2.2 provide a simple but powerful understanding of how observing system uncertainties will affect decadal climate change trends. The most important result is that observing system errors should be viewed relative to natural variability as a reference. As the magnitude of uncertainties fall below that of natural variability, they will rapidly become insignificant for climate trend errors. As the time scale for uncertainties becomes shorter than natural variability, they also become less significant. The framework discussed in Section 2.1 (and derived in Appendix A) provides a method to rigorously consider a wide range of error sources: calibration, accuracy, orbit sampling, reference inter-calibration uncertainty, and instrument noise. Mission design can then successfully trade cost and value across these error sources.

Finally, recall that Equations 2.1 and 2.2 showed that climate trend accuracy, which is related to the ratio U_a, and time to detect trend, which is related to the ratio U_t, are tightly related. For values of U_a near 1, their relationship simplifies to Equation 2.3. Another way of saying this is that if the CLARREO observing system goal is for decadal trend accuracy to be no more than 20% larger than that determined from a perfect observing system, then the time to detect trends with a CLARREO-like system will take no more than $0.67 \times 20\% = 13.4\%$ longer than with a perfect observing system. This therefore provides a simple relationship between the two science goals. For the CLARREO MCR Baseline Mission, the Level 1 requirements specify trend accuracy within 20% of a perfect observing system and time to detect trends within 15% of a perfect observing system.

The final decision is how to use climate trend accuracy as a metric in the science value matrix. The science value equation, Equation 3.1, requires a metric that increases with increasing accuracy, and a metric that reduces to zero as accuracy becomes so poor that CLARREO's value to the climate observing system is lost. Currently, 1.0 is assigned to the accuracy factor if the full CLARREO mission Level 1 Requirement of trend accuracy within 20% of a perfect observing system is met. This accuracy level is assumed to be 100% of the capability value. As accuracy in decadal change trends reduces below this, the accuracy value factor is reduced proportional to the loss of accuracy. In particular, the trend accuracy value factor is defined as:

$$F_{ta} = \frac{1.2 \times U_a}{U_{clarreo}} \,. \tag{3.2}$$

As the CLARREO MCR Level 1 requirement goal is to be within 20% of a perfect observing system, $F_a = 1.0$ when the trend accuracy requirement is met, $F_{ta} > 1.0$ when CPF measurements achieve trend accuracy better than requirement, and $F_{ta} < 1.0$ when CPF measurements exceed the 20% accuracy limit.

The accuracy values used in Table 3.1 are determined from the CLARREO SDT studies and include calibration absolute accuracy, orbit sampling error, and instrument noise. The accuracy factor is the same independent of whether CLARREO or CPF uses a spectral benchmarking approach or reference inter-calibration. Reference inter-calibration error can be added, but the studies indicate that this error is equal to or lower than orbit sampling error. In general, the CLARREO and CPF decadal change accuracy is dominated by the instrument absolute accuracy for global annual time scales. Orbit sampling error becomes more important at zonal and regional spatial scales and at seasonal time scales. This difference is a result of the fact that calibration error is independent of the space/time scale, while the errors from natural variability and sampling both increase as space/time scale reduces. Orbit sampling studies have shown that natural variability and orbit sampling error increase roughly proportionally. For example, natural variability at zonal annual time scales are three times larger than that at global annual time scales. As a result, the effect of calibration uncertainty is largest for global annual time/space scales. For many purposes, however, the global annual values are some of the most critical measures and are the first to show anthropogenic signals given their lower natural variability. This is true for everything from global average surface temperature to the impact of feedbacks on climate sensitivity. As a result, the accuracy metric used in the science value matrix uses global annual trend accuracy.

The trend accuracy factor has been determined separately for each instrument: spectral RS, spectral IR, and RO. This allows for different calibration accuracies, orbit sampling, and instrument noise for each instrument and mission design to be accounted for. The factor is slightly greater for the IR than for the RS because of lower fractional sampling errors in the IR as well as a somewhat smaller absolute calibration error. For calculation of each science objective's science value, the maximum trend accuracy factor is used out of the three CLARREO measurement types: spectral IR, spectral RS, and RO.[3] Note that because the CPF includes the RS spectrometer only, its trend accuracy factors for variables that require either IR observations or the combination of RS and IR measurements, are zero.

Climate Record Length Factor

The trend accuracy metric discussed above is relative to a perfect observing system. While this is a critical part of climate trend accuracy, Equation A.2 shows that the length of the climate record is also a key factor in determining the accuracy of trends – for both a perfect observing system and for a CLARREO-like system. As follows from Equation A.2, the uncertainty of climate trends, δm, will scale as $(\Delta t)^{3/2}$. As explained in Leroy et al. (2008), the reduction in trend error with length of record is a result of two very different factors. First, a linear dependence on record length occurs as a result of increasing climate trend signal magnitude with length of record. Second, there is a $\sqrt{\Delta t}$ that is a reduction in natural variability with averaging over an increasing number of autocorrelation time periods.

Here, if it is assumed that there will be multiple CLARREO missions, the first would contribute to the linear component by achieving the absolute accuracy and time in orbit needed to overcome gaps in the climate record. For example, a 30-year trend could be achieved by using the first 5 years of the CLARREO record, followed by another 5 years of equivalent data 30 years later. In this sense, the linear record length component is dependent on getting the first CLARREO up to start the record, but is then dependent primarily on whether follow-on missions are flown. In that sense, the first mission record length is independent of this linear component.

The second factor, the $\sqrt{\Delta t}$ component, however, is relevant to the first CLARREO mission.

[3] For RO water vapor science objective, the accuracy is listed as low, primarily because of low information content. The science value for this observation is from the IR instrument with a much smaller contribution from the RO observation.

Consider, for example, if the first CLARREO was launched and only achieved 1 month or 1 year of data (as is the current lifetime of the CLARREO Pathfinder). Even though highly accurate, it would not anchor the long-term record well because of high natural variability. As a result, in the science value matrix for the first two CLARREO missions, the square root dependence of record length is included. In particular, the climate record length metric is chosen as

$$F_{crl} = \sqrt{\Delta t}\,, \tag{3.3}$$

where Δt is the number of years of CLARREO data with a 70% likelihood of survival on-orbit. Using this metric, the length of the initial CLARREO record (for example, the CLARREO Pathfinder) will be accounted for in determining the accuracy of the climate trends that can be achieved by the mission, even in the long term.

The value of Δt is determined using the normal engineering estimates of the likelihood of launch success, spacecraft survival, and instrument survival. The failure rates of instruments and spacecraft are controlled by the amount of redundancy built into the systems, especially for key electronics components. For example, single string electronics will be less reliable than redundant electronics. This allows a cost/value trade for the CLARREO mission for instrument and spacecraft reliability, especially selected redundancy of key components. As for other missions, the CLARREO failure rates of instruments, spacecraft, and launch vehicles are assumed to be independent. The 70% likelihood in the CLARREO Pathfinder mission (Table 3.1) that the RS spectrometer survives is 2 years. This gives a value of $F_{crl} = 1.4$.

For many CLARREO science objectives, only one of the CLARREO instruments is required (e.g. the IR spectrometer for water vapor profile or the RS spectrometer for SW Cloud Feedback); while for others (e.g net cloud feedback) both reflected solar and infrared spectrometers are required. The value of Δt is calculated accordingly, with independent failure rates assumed for each instrument. If there is a time when more than one CLARREO spacecraft is in orbit, the value of Δt accounts for the joint probability that multiple spacecraft and instruments survive if the science objective requires it. Alternatively, if only one instrument is required to survive, then the value of Δt accounts for the fact that one instrument of either spacecraft is sufficient.

Risk Factor

Any science value estimation should consider risk as an element of its science value metrics. One example of risk is technological risk. All new instruments, including those that are part of the CLARREO and CLARREO Pathfinder missions, will have some level of risk in demonstrating the viability of new technologies in-orbit. One of the key objectives in the ESTO IIP investigations related to CLARREO is to reduce this risk from moderate to low values. The CLARREO engineering team has evaluated the risks in the current IR, RS, and RO instrument designs and has not found a large difference in the risk factor of these instruments. As a result, this factor, F_r, is currently left at 1.0 for all instruments, but could be adjusted in the future.

Total Science Value

After computing the Mission Value (far right column in Table 3.1) for each Science Objective, the Total Mission Value can be computed by taking the sum of the Science Objective Mission Values. Although this value is arbitrary, it is helpful to compare this value to other mission options as a way to quantify their relative science values. The CPF mission concept (i.e. including the CLARREO RS spectrometer only to be mounted on the ISS for one year) captures 16% of the CLARREO MCR Baseline Mission science value. Applying the factors above to a CPF mission concept that only includes the IR spectrometer has a slightly smaller science value at 12% compare to the CLARREO MCR Baseline Mission concept. If both the RS and IR were included in the CPF mission concept, the mission could capture 37% of the science value compared to the CLARREO MCR Mission. The IR only and RS only mission concepts do not add linearly because there are some science objectives that need both measurements together. Without both the RS and IR, for example, there is no added benefit to the net cloud feedback.

3.4 CLARREO Pathfinder Mission Timeline

The CLARREO Pathfinder was included in the FY2016 NASA President's Budget Request and was ultimately included in the omnibus package that was passed in December 2016. The CPF team received the Authority to Proceed (ATP) to conduct pre-Phase A activities for the CLARREO Pathfinder mission, leading to a Key Decision Point "A" (KDP-A) review to be held no later than the end of September 2016. Upon approval at KDP-A the CLARREO Pathfinder project may proceed to conduct Phase A activities (formulation and requirements definition). The remainder of the currently planned mission timeline is shown in Figure 3.2, extending from the date from which the CPF team received the ATP through the currently stated end of the mission, which is the end of FY2022.

The timeline shown in Figure 3.2 shows activities categorized into four groups: mission milestones and instrument-related, launch vehicle-related, and operations activities. The first major hurdle to be overcome by the team after first receiving funds is to pass its Mission Concept Review (MCR). Upon successful completion of its MCR, the project will be permitted to pass the Key Decision Point-A (KDP-A) and enter Phase A. There are several other reviews and KDPs in addition to building the instrument, developing flight software and several other important activities that the team must pass to successfully reach the point at which the instrument will be ready for launch to the ISS, which is currently planned for the last quarter of 2020. Following the launch, installation on ISS, instrument commissioning, and one-year operational period, there is one additional year within the project plan for data analysis support. As currently planned, the CPF is due to end at the end of FY2022.

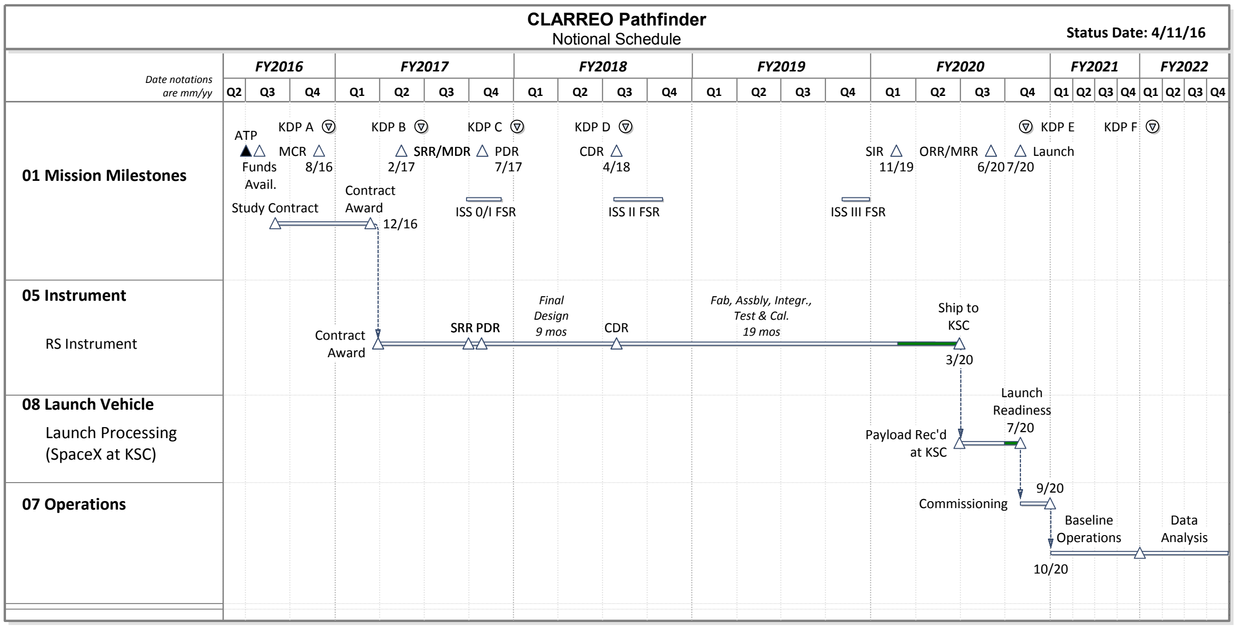

Figure 3.2: The notional schedule for the CLARREO Pathfinder Mission from the start of the project, defined as the date the Authority to Proceed letter was provided from NASA HQ, to the end of the data analysis one-year period.

4 CLARREO Pathfinder Instrumentation & Mission Requirements

4.1 Mission Requirements

The CLARREO Pathfinder Mission is considered a Class-D mission and comprises of a reflected solar instrument that will be hosted on the International Space Station (ISS) beginning in the 2020 timeframe. The ISS has a 51.6° inclination and 400 km altitude orbit. Upon successful delivery to the ISS, the CLARREO Pathfinder RS instrument will be allowed to outgas and undergo instrument checkout and evaluation prior to the commencement of the prime mission phase for a period that is expected to last no longer than 2 months. Mission, instrument, and data product requirements are outlined below.

The CLARREO Pathfinder Mission is a technology/technique demonstration mission. Therefore the Baseline Mission Objectives and Level-1 Threshold Requirements are defined in terms of the technology demonstration.

The CLARREO Pathfinder Mission Baseline Mission Objectives are as follows:

1. Demonstrate the ability to conduct on-orbit SI-Traceable calibration of measured scene spectral reflectance with an advanced accuracy over currently operational sensors using a reflected solar spectrometer flying on the International Space Station.
2. Demonstrate the ability to use the improved accuracy to serve as an in-orbit reference

spectrometer for inter-calibration of other key satellite senosors across the reflected solar spectrum (350 – 2500 nm).

Mission success is defined at the CLARREO Pathfinder Mission meeting its threshold requirements, stated as follows:

1. Demonstrate in-orbit new solar attenuator technologies for higher accuracy calibration within the reflected solar bands (350 – 2500 nm).
2. Demonstrate the solar and lunar cross calibration approach.
3. Demonstrate improved methodologies for reference inter-calibration of VIIRS and CERES.
4. Demonstrate new gimbal pointing ability to match the entire instrument scanning view of instruments like CERES and VIIRS for reference inter-calibration.

4.1.1 Requirements for Reflected Solar Measurements

The threshold requirement for the CLARREO Pathfinder RS instrument includes inter-calibration of the VIIRS and CERES instruments. The CLARREO Pathfinder will perform reference inter-calibration for any of these bands for which there is a suitable signal to noise level and sufficient sampling of high-accuracy observations that are matched in time, space, and viewing angles to overcome the random error sources from instrument noise and imperfect data matching.

The SI-traceable accuracy advancement will be determined relative to ensemble means and for spectral reflectance relative to the global mean reflectance. To calibrate the spectrometer relative to SI-Traceable standards, the CLARREO Pathfinder RS instrument will have the ability to observe the sun and the moon as stated in Section 4.2. It will also take spectral reflectance measurements of the Earth at nadir to demonstrate its inter-calibration capabilities.

To achieve reference inter-calibration of other reflected solar sensors, the CPF RS instrument will provide constraints to the effective offset, gain, non-linearity, and sensitivity to polarization of a target sensor.

4.1.2 Requirements for Data Products

CLARREO Pathfinder is a technology/technique demonstration mission and therefore will only produce Level-1 data products. Level-0 data from the CPF RS instrument will be collected and archived at a data center, the location of which has yet to be identified. Additionally, these Level-0 data will be processed into Level-1 products, which will also be archived at a data center. The Pathfinder budget does not support Level 2 and Level 3 processing. Level 4 processing is limited to that sufficient to demonstrate inter-calibration for the CERES and VIIRS. Within one year following the end of the one-year prime mission operations period the CPF instrument team will submit their results with Level 4 processed data, demonstrating the achievement of advances in on-orbit SI-traceable accuracy and inter-calibration of CERES and VIIRS to appropriate peer-reviewed journals.

If Pathfinder is judged highly successful, meaning that the team has advanced the technology development and delivered useful science, NASA HQ may decide at a later time to fund processing of the Pathfinder Level 0 observations to provide the full CLARREO mission Level 1 through Level 4 data products. All data that will be archived at data centers will be available to the community for independent verification of the CPF instrument team's results.

4.2 Reflected Solar Instrument Concept

Summaries of the CLARREO Pathfinder (CPF) RS instrument requirements can be found in Section 4.1.1 and Figure 3.1, and details on how these requirements were determined can be found in Section 2. The RS instrument design concept, shown in Figure 4.1, is driven by these requirements and is similar to the RS instrument concept for the full CLARREO mission. The RS spectrometer spans 350 nm to 2300 nm and has a spectral sampling resolution of 4 nm and spectral resolution of 8 nm. The two focal planes cover two spectral ranges, 350 – 640 nm and 600 nm – 2300 nm and are implemented as two individual spectrometers.

The Earth-viewing measurement signal can vary by factors of 2 to 10 due to the signal magnitude's dependence upon a wide variety of parameters including solar zenith angle, spectral band, and scene type, which can range from very dark (e.g. clear-sky ocean) to very bright (e.g. dry desert area or deep convective clouds). The RS instrument must be designed to handle such a large dynamic range and maintain the ability to satisfy the rigorous SI-traceable accuracy requirements needed for mission success.

On global scales such an accuracy requirement acts to reduce sampling biases on the large temporal and spatial scales relevant to climate change studies. A primary motivation for the spectral range, resolution and sampling requirements is the planned activity to inter-calibrate with shortwave broadband (e.g. CERES) and narrowband (VIIRS) radiometers. The 300 m ground-field-of-view (GFOV) requirement is necessary to obtain a high-quality cloud mask, and the spatial coverage is driven by the science objective to obtain a RS climate benchmark on a global scale with nadir RS measurements. Reference inter-calibration will be enabled by the instrument's ability for the boresight to be pointed along particular lines of sight with the fields of view of operational target sensors as shown in Figure 2.3.

The CPF RS spectrometer's measurements of Earth-reflected radiance will be used to calculate reflectance using solar and lunar irradiance measurements, also made by the RS spectrometer [*Wielicki et al.*, 2013]. The current operational plan for the RS instrument is to determine the ratio of the Earth-reflected radiance to the solar irradiance measurement. The geometric differences between an Earth-viewing radiance measurement and a solar irradiance measurement requires the retrieval of a directional-hemispheric reflectance. Thus, the RS sensor will function like a band-ratio radiometer. The instrument is based on an Offner imaging spectrometer design, which is capable of limiting spectral smile on the focal plane.

The instrument will operate as a push-broom imager with a reliance on heritage hardware, reduction of sensor complexity, and solar- and lunar-source based calibration.

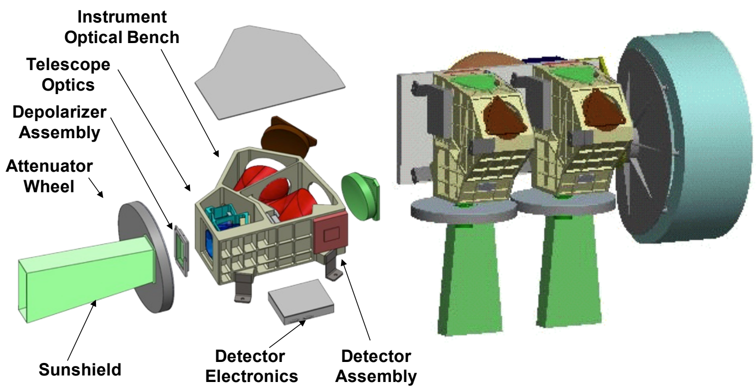

Figure 4.1: RS spectrometer concept design, showing details of a single spectrometer (left) with an exploded image and the dual spectrometer system as it might appear on the spacecraft (right).

Among the critical aspects of the CPF instrument concept is its ability to satisfy the unprecedented radiometric calibration accuracy requirement. Such a requirement is an improvement on the scale of 5 to 10 times compared to past and existing RS sensors. The sensor signal-to-noise ratio (SNR) for a single sample are defined for a radiance measurement based on a reflectance of 0.3 and solar zenith angle of 75°. The required SNR is > 33 for wavelengths 380 – 900 nm and an SNR > 20 for wavelength ranges 320 – 380 nm and 900 – 2300 nm. Figure 4.2 demonstrates the measurement and calibration approach for the reflected solar spectrometer and its use of the moon as a reference for stability in orbit, the sun with multiple attenuators to verify instrument nonlinearity of gain across the Earth-viewing dynamic range, and the ability to directly scan deep space to verify instrument offsets [*Espejo et al.*, 2011, *Fox et al.*, 2011].

Spectral response is verified using solar spectral absorption line features. One of the unique aspects of this instrument compared to other operational instruments is its ability to point the entire instrument at Earth, the sun (every 2 weeks), the moon (monthly, at 5 to 10° phase angle), and deep space. This eliminates the need for scanning mirrors with angle-dependent calibration uncertainties and allows the use of depolarizers to reduce polarization sensitivity to the required accuracy level over the entire spectral range [*Lukashin et al.*, 2015]. Scanning the instrument view across lunar and solar disks provides images suitable for verifying stray light performance. Finally, any future improvements in the absolute reflectance of the lunar surface can be used to tie the CLARREO solar spectrometer results to future improvements in calibration beyond the CLARREO lifetime, even if these improvements come several decades after its launch [*Kieffer*, 1997, *Kieffer and Stone*, 2005]. Note that the calibration of the reflected solar is in reflectance units. Conversion to absolute radiance can be done using the spectral total solar irradiance provided by instruments, such as TSIS, with expected absolute accuracy of 0.25% [*Richard et al.*, 2011].

4.2.1 CLARREO Pathfinder RS Instrument Calibration

Calibration SI-traceability is the cornerstone of the success of the CLARREO mission and a key objective of the CLARREO Pathfinder technology demonstration. Successful demonstration of SI-traceability of CPF accuracy requirements on orbit requires both a detailed preflight calibration and a transfer of that calibration to orbit.

The instrument design relies on a direct solar view as part of the on-orbit calibration approach. The solar irradiance and Earth-reflected radiance are combined with knowledge of sensor optical geometry to retrieve at-sensor reflectance. To observe both the solar irradiance and Earth-reflected radiance in the same dynamic range, the RS instrument must be able to reduce the solar irradiance to a level comparable to the Earth-reflected radiance, a difference on the order of 50,000. The attenuator approaches being evaluated to achieve this objective include a single pinhole aperture, neutral density filters, a collection of pinhole apertures, or some combination of these concepts. More than one attenuator approach is being studied for consideration to satisfy an additional CLARREO goal to rely on multiple, independent calibration approaches.

The attenuators require careful ground testing evaluation and are a source of uncertainty on orbit should attenuator degradation occur. Evaluating the attenuators on orbit involves coordinated solar and lunar views. The moon has sufficiently low brightness to permit measurements without the use of the attenuators, which allows coupled lunar and solar views to verify proper operation of the attenuators. Instrument nonlinearity will be evaluated using a range of attenuators while observing the sun.

The primary sources of error in transferring prelaunch calibration to orbit is expected to be changes in stray light behavior and polarization sensitivity.

The solar irradiance ($E_{solar,\lambda}$) measured by CLARREO can be written in terms of the sensor output while viewing the sun ($S^{solar}_{i,\lambda}$) and responsivity ($R'_{i,\lambda}$) of the ith detector and in a given wavelength band, λ, as shown below.

$$E_{solar,\lambda} = \frac{\sum_{\substack{x_{solar}\\ y_{solar}}} S^{solar}_{i,\lambda}(x'_{solar}, y'_{solar})}{R'_{i,\lambda} T_{attenuator} A_{attenuator}} \tag{4.1}$$

$T_{attenuator}$ is the transmittance of the attenuator used in viewing the sun, and $A_{attenuator}$ is the area of the attenuator's aperture. The summation over x_{solar} and y_{solar} serves to integrate the output from a single detector over the full solar disk needed to measure solar irradiance.

The Earth-reflected radiance measured by CLARREO can be written as

$$L^{earth}_{i,\lambda} = \frac{S^{earth}_{i,\lambda}}{R_{i,\lambda} A_{sensor} \Omega_{sensor}} \tag{4.2}$$

where A_{sensor} is the area of the sensor's entrance pupil, Ω_{sensor} is the solid angle of the sensor's

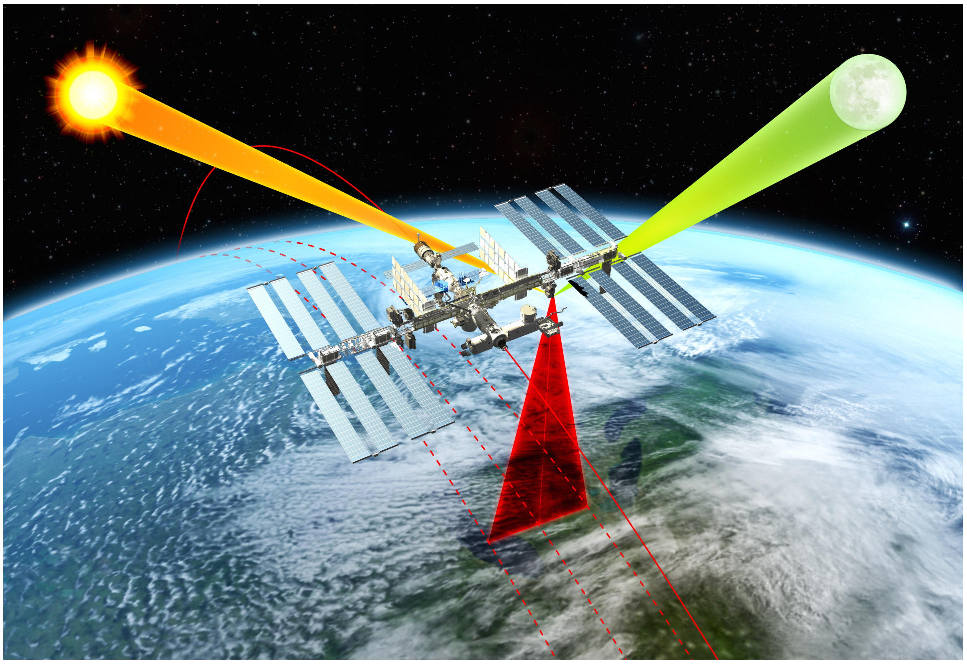

Figure 4.2: Illustration showing the RS instrument calibration concept: verification of nadir spectral reflectance accuracy relies on rotating the entire instrument to view the moon at constant phase angle as a stable reflectance source (similar to SeaWiFS), the sun in combination with filters and precision apertures for nonlinearity determination, and the use of depolarizers to control polarization sensitivity.

collection field of view, $R_{i,\lambda}$ is the detector response, and $S_{i,\lambda}^{earth}$ is the spectrally-resolved signal from the ith detector while viewing Earth. The Bidirectional Reflectance Distribution Function (BRDF) is determined by the ratio between the Earth-reflected radiance ($L_{i,\lambda}^{earth}$, Eqn. 4.2) and the solar irradiance ($E_{solar,\lambda}$, Eqn. 4.1).

$$BRDF_{i,\lambda}^{earth} = \frac{L_{i,\lambda}^{earth}}{E_{solar,\lambda} cos\, \theta_0} \tag{4.3}$$

$$= \frac{S_{i,\lambda}^{earth}}{R_{i,\lambda} A_{sensor} \Omega_{sensor}} \frac{R'_{i,\lambda} T_{attenuator} A_{attenuator}}{cos\, \theta_0 \sum_{x_{solar}}^{y_{solar}} S_{i,\lambda}^{solar}(x'_{solar}, y'_{solar})} \tag{4.4}$$

where θ_0 is the solar zenith angle at the TOA. It is assumed that any temporal changes in response between the solar and Earth views, $R'_{i,\lambda}$ and $R_{i,\lambda}$, respectively, will be minimal and changes in solar irradiance between the Earth and solar view will also be minimal. If these differences are negligible, then detector response for the sun and Earth view cancels out. In this case, the absolute radiometric calibration is not used for the BRDF retrieval, but it is required for establishing SI-traceability.

Ensuring SI-traceability and adequate accuracy requires evaluation of sensor performance on orbit and it requires a traceable error budget. The basis of the traceability for the CLARREO Pathfinder RS instrument is a high-fidelity sensor model developed from prelaunch characterization data coupled with on-orbit absolute solar irradiance measurements to show the sensor did not change as it was launched into orbit. Disagreement between measured and predicted values of solar irradiance imply that the sensor model requires modification. Solar and lunar views provide information regarding the optical quality and temporal changes of the sensor. The sensor model can be thought of as the numerical abstraction of the physical instrument, encapsulating knowledge of both the optical physics and empirical results gained from laboratory analysis. Disparities between laboratory results and model predictions guide model improvements. This is a continuous process that ultimately yields a sensor model ready for use after launch as illustrated in Figure 4.3.

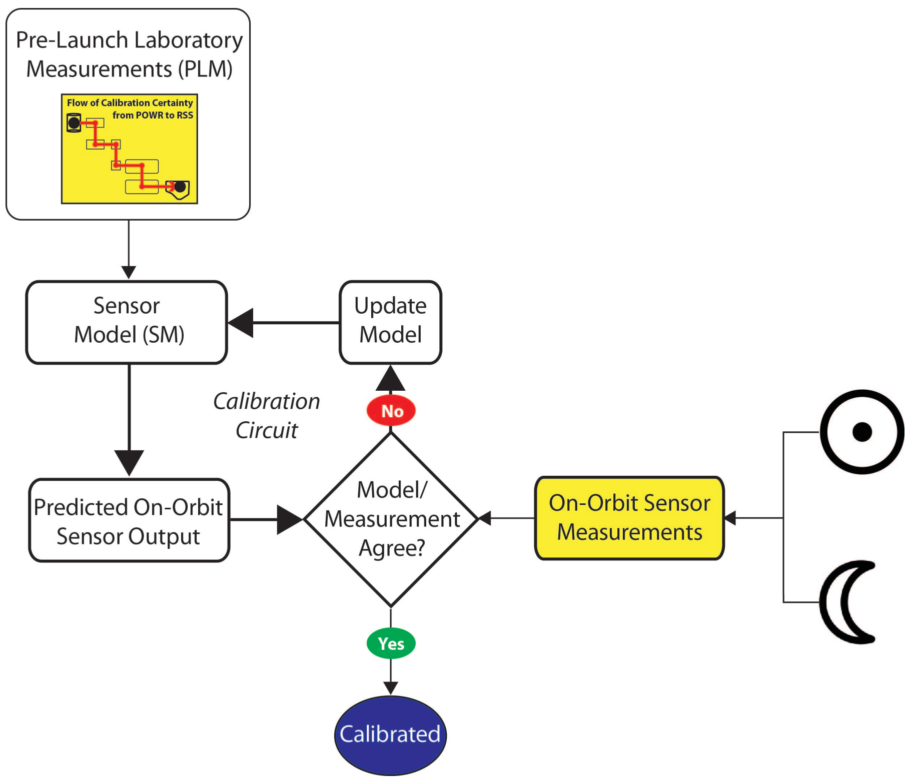

Figure 4.3: Flow diagram showing the key to the RS on-orbit calibration: the prelaunch, SI-traceable calibration.

A critical part of the calibration is developing SI-traceable data by characterizing the sensor to SI-traceable, absolute radiometric quantities during pre-launch calibration to the SI quantity power in Watts (prelaunch calibration box in Figure 4.3). Pre-launch absolute calibration includes both irradiance and radiance modes and the determination of geometric factors for conversion to reflectance. The end result of the prelaunch calibration is sufficient data to develop a sensor model capable of predicting the solar, lunar, and planetary/stellar sources planned for on-orbit calibration. Agreement between pre-launch and on-orbit values (as shown in Figure 4.3) implies the system is calibrated to a level traceable to the pre-launch SI measurements. Disagreement implies the sensor model requires improvement based on the on-orbit data, including an additional set of characterization measurements. Solar and lunar views provide information regarding temporal changes in the sensor once on-orbit traceability is established. Thus, the key to the RS on-orbit calibration is the prelaunch, SI-traceable calibration.

Evaluation of sensor performance on orbit uses combined calibration, validation, and verification activities. One approach planned for validation of the RS on-orbit calibration is comparison to ground-based measurements propagated through the atmosphere to predict at-sensor radiance. Another radiometric calibration/validation activity will be comparisons to other sensors (e.g. airborne sensors). The main difficulty with validation for CLARREO RS will be ensuring that the validation data sets also have sufficient radiometric quality.

4.2.2 Operational Requirements for Lunar Verification

The CLARREO Pathfinder Reflected Solar (RS) instrument calibration concept includes monthly observations of the moon to verify radiometric calibration stability on orbit (Section 4.2.1). The primary RS calibration relies on direct measurements of the sun, which must be obtained with attenuators to reduce the solar irradiance. Because attenuators are not required when viewing the moon, lunar observations will be used throughout the mission to evaluate the performance of the solar attenuators in orbit. This is enabled by the inherent stability of the lunar surface reflectance.

The operations plan for the RS lunar verification observations specifies that measurements of the moon will be acquired at phase angles between 5°and 10°. Although this range is relatively small, the lunar irradiance cannot be considered constant across this range. As an example, Figure 4.4 shows irradiance spectra from one night of ground-based observations during which phase angle changed from 6.65° to 9.55° over about 9 hours. The difference between the two spectra ranges from 10% to 12% depending upon the wavelength band. Generally, lunar views acquired from orbit are dependent on which hemispheres of the moon are illuminated and viewed, referred to as the lunar librations. Consequently, CPF RS lunar measurements must be normalized to remove geometry-driven differences in brightness before the measurements can be used to assess instrument calibration stability. Normalization is done using the reference lunar spectral irradiance generated for the specific measurement conditions (phase and librations) by the USGS ROLO (Robotic Lunar Observatory) lunar irradiance model [*Kieffer and Stone*, 2005]. These model-generated reference spectra can be used to develop normalization factors, or to correct the observations to a standard geometry (specified phase and librations).

The CLARREO Pathfinder RS instrument is likely to be an imaging spectrometer with a ∼10° cross-track FOV. From low Earth orbit, the moon's diameter subtends about 0.5°. To make a lunar irradiance measurement, the entire disk must be spatially sampled, which for an imaging spectrometer typically means scanning it in the along-track direction. Generating the irradiance from the scan data involves concatenating the scan lines into a spectral image, then spatially summing the radiance pixels and multiplying by their IFOV:

$$E_m = \Omega_p \sum L_i \tag{4.5}$$

where E_m is the measured lunar irradiance, Ω_p is the pixel IFOV in steradians, L_i is the radiance measure of the ith pixel, and the summation is over all pixels on the moon's disk.

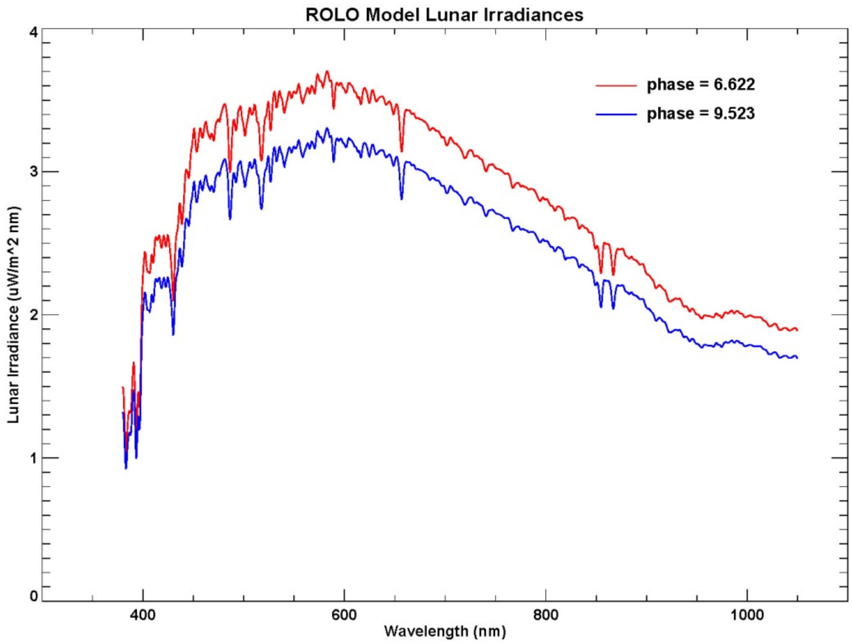

Figure 4.4: ROLO model-generated lunar irradiance spectra produced for a ground-based spectrometer. The observation times differ by 9 hours and 21 minutes, and the phase difference is 2.9°. The irradiances differ by 10% to 12%, so the moon cannot be considered constant between 5°and 10° phase angles.

Recommended best practices suggest oversampling the moon in the along-track direction and underfilling the cross-track FOV. To obtain accurate irradiance measurements, correction factors for the disk oversampling must be determined carefully. This requires accurate knowledge of instrument pointing and spacecraft position, velocity, and attitude, sampled at frequencies higher than the scan line acquisition rate. The moon must be scanned at a uniform rate over the lunar disk, so that the oversampling rate is constant for the entire scan. This imposes stability requirements on the slew rates of the instrument gimbal and the spacecraft attitude during moon imaging. The corrections for oversampling are typically applied to the irradiance measurements from spectral images prior to normalization using output from the lunar model.

CLARREO Pathfinder engineering studies continue to be conducted to optimize acquisitions of the moon by the RS instrument, directed toward obtaining the highest accuracy lunar irradiance measurements. These studies are taking into account such limitations on the observability of the moon by the mission configuration, such as the instrument's location on the ISS (Section 3.1).

The summation of spectral images to calculate irradiance (Eqn. 4.5) involves working with radiometrically calibrated radiance pixels and having corrections applied for detector artifacts such as dark-level and bias offsets, flat-fielding, and response linearity. Because the moon is an extended source viewed against the near-zero radiance background of deep space, in many cases detector dark-level offsets can be evaluated independently and verified using the over-sampled regions of the observations. Additionally, the high-contrast edge of the illuminated moon limb can be used to evaluate light scattering by the instrument optics, which must be accounted for in the image processing to determine irradiance.

Accurate irradiance measurements depend on precise pixel response equalization, or flat-fielding. Depending on the duration of the orbit eclipse periods, multiple views of the moon may be acquired for each observation opportunity, potentially scanning with different parts of the detector array. However, it is not operationally practical to acquire a complete spatial sampling of the moon in every spatial element (i.e. all detectors). Since the moon is a relatively dark target (mean reflectance is 0.11 at 550 nm), lunar irradiance measurements are sensitive to detector response linearity at the lower end of the dynamic range. Thus, a thorough characterization of sensor linearity is essential for successful lunar calibration operations. It is possible to use the moon to assess linearity on orbit; however, there are a number of complicating considerations involved with this type of analysis.

Practically, the lunar irradiance measurements acquired by the CPF RS instrument, when compared with the corresponding lunar reference values, each constitute a snapshot radiometric calibration of the RS sensor. Collecting these comparisons into time series can reveal the temporal stability of the instrument radiometric calibration independently of the performance of the solar attenuators. Given a sufficiently long time series, the uncertainty in this temporal trending can be reduced to under 0.1% per year (e.g. Sea-WiFS, [*Eplee et al.*, 2012]). This metric is evaluated from fitting the measured irradiances to the reference irradiances as a function of time, where each measurement and model value has an associated error. Error in the irradiance measurements are developed from characterizations of the scan sequence, pixel conversions to radiance, and spectral image processing to irradiance. The reference value errors arise from residual geometric dependencies in the lunar model; for the phase angle range of 5°–10°, the relative error is no more than a few tenths of a percent. Sensor response trends derived in this way are not affected by the absolute accuracy of the lunar model as a first-order dependency.

To use the RS lunar irradiance measurements for on-orbit evaluation of the solar attenuator performance requires knowledge of the absolute reflectance of the moon, spatially integrated over the lunar disk, for the conditions corresponding to the lunar views. This can be determined using the USGS ROLO lunar irradiance model and a solar spectrum. However, a major caveat of this process is the uncertainty in the absolute scale of the ROLO model, which currently cannot be verified against radiometric standards to better than 5–10%. However, the absolute offsets of the lunar model are consistent across its spectral and viewing and illuminated geometry ranges, enabling a verification strategy that references a set of baseline lunar measurements acquired at the earliest opportunity upon the CPF achieving orbit. These initial observations are used to establish a spectrally-resolved offset to the lunar model that can be considered constant through the mission lifetime. The validity of this method is substantiated by the time invariance of the lunar reflectance.

It should be noted that future improvements to the lunar model absolute scale can be applied retroactively to the operational RS lunar measurement datasets, and several projects for refining the USGS lunar model are ongoing, with the common goal of improving and/or verifying the model's absolute accuracy and assuring SI traceability. In a longer view, it is recognized that a lunar observation dataset acquired by CPF could potentially contribute to a future characterization of lunar absolute reflectance, presuming the RS instrument operates within its absolute accuracy specifications for reflectance measurements (Section 4.1). This supplemental CPF task would require expanding the range of lunar phase angles observed by the RS instrument, and developing a corresponding set of operational requirements to support these observations.

4.3 CLARREO Pathfinder Technical Readiness

The CLARREO Pathfinder reflected solar spectrometer instrument technology is mature, having achieved a Technical Readiness Level of 6. The RS spectrometer instrument has achieved this high level of technical readiness by CLARREO team members successfully competing for funding through the NASA Earth Science Technology Office (ESTO) Instrument Incubator Program (IIP), developing successful collaborative relationships with researchers at the National Institute of Standards (NIST), and developing a RS Calibration Demonstration System (CDS) at NASA GSFC. In addition to the efforts that will directly contribute to the success of CPF, the CLARREO team has also worked to increase the maturity of the IR and GNSS-RO instruments. Here, we will be discussing the technical readiness of the RS spectrometer instrument. For discussion of the IR and GNSS-RO instrument development, see the CLARREO Science Team Summary Report.

4.3.1 NASA Investments in CLARREO Technology

Within the past decade, NASA ESTO has carefully managed technology projects and enabled the building and validating of early versions of the instruments and components needed for such a mission as CLARREO. In many ways, the development of these early investments enabled the designation of CLARREO as a mission concept in 2007. ESTO investments made since 2007, adopted by the CLARREO Science Definition Team, are summarized in Figure 4.5, and amount to ∼\$18M total. The earlier ESTO investments relevant to the CLARREO mission amount to ∼\$8M total. What follows is the list of these key technologies with a focus specifically on CLARREO Pathfinder mission requirements.

◇ Initiated in 2008, the Hyperspectral Imager to Meet CLARREO Goals of High Absolute Accuracy and On-Orbit SI Traceability project seeks to design and construct an advanced, high accuracy hyperspectral imager, investigate attenuation methods, and validate the solar cross-calibration approach for the CLARREO mission concept.

◇ For the 3-year term of the ROSES-selected CLARREO Science Definition Team (2011–2014), Calibration Demonstration Systems (CDS) in the RS and IR were funded at NASA GSFC and NASA LaRC, respectively. The total funding amounted to ∼\$3M. The scope of each CDS was to design technology demonstrators for each spectrometer in the CLARREO mission concept and to achieve the comparable instrument performance specifications. The calibration process and its SI-traceability was developed in collaboration with NIST.

◇ Between 2010 and 2014, NIST supported CLARREO mission development, focusing on establishing high-accuracy calibration and the SI-traceability of relevant measurements from

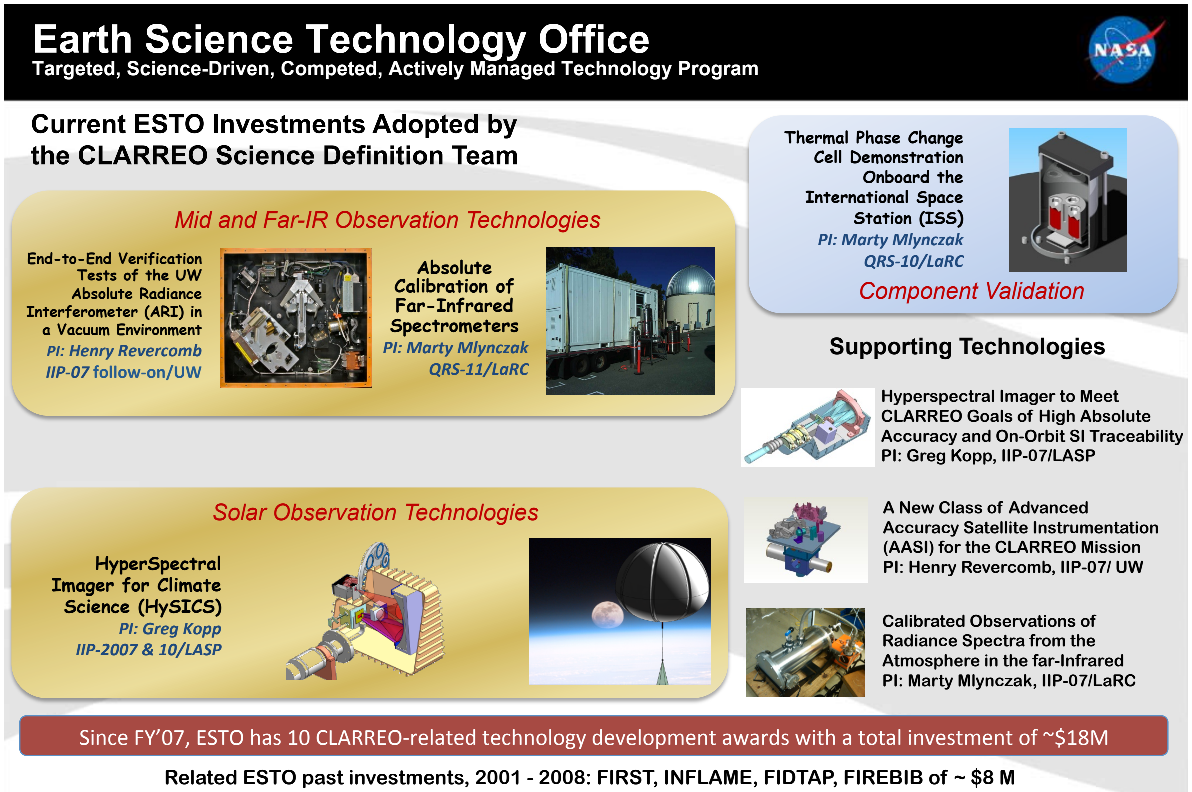

Figure 4.5: NASA ESTO investments in CLARREO-relevant technology have totaled almost \$18M.

space. These activities were supported in part through NASA funding agreements totaling ∼\$650K and, in part, through NIST climate initiative internal funding of ∼\$1.2M. In 2013, NIST collaborators also reviewed the design and performance of both the RS and IR CDS.

4.3.2 SOLARIS Calibration Demonstration System at NASA GSFC

The Reflected Solar Calibration Demonstration System (CDS) is specially designed for the Reflected Solar (RS) spectrometer component of the CLARREO mission concept, and is intended to achieve the same instrument performance specifications as the full CLARREO and CLARREO Pathfinder spectrometers (CPF requirements summarized in Table ??); however, the RS CDS also supports the success and development of the CLARREO Pathfinder RS spectrometer. The RS CDS consists of two major subsystems: (1) the SOlar, Lunar for Absolute Reflectance Imaging Spectroradiometer (SOLARIS), and (2) the associated calibration support equipment needed to evaluate the spectrometer's calibration. Considering both as part of the CDS emphasizes that reducing the risk of achieving on-orbit CLARREO and CLARREO Pathfinder calibration requirements relies on both the sensor design as well as developing the laboratory characterization. The goals of the SOLARIS CDS is to create and check calibration protocols and methods, demonstrate the path to SI-traceability (source and detector standards), and prove the ability to derive reflectance via a view of the Sun and Earth's scene. The instrument build and testing takes place primarily at the NASA Goddard Space Flight Center.

A silicon-based detector, coupled with Indigo 9803 640×512 pixel read-out integrated circuits (ROIC), is the current baseline for the sensor covering the wavelength range from 320 nm to 640 nm. The "red" spectrometer is based on MgCdTe detectors coupled to the same ROIC and samples the 600 nm to 2300 nm spectral range. Polarization sensitivity is minimized for both systems to levels below 0.5% through depolarizers placed in front of the telescope. Solar irradiance is attenuated through the use of a single pinhole aperture, neutral density filters, a collection of pinhole apertures, or various combinations of the three. A silicon-based detector has been fully evaluated (as described below) and has been integrated with a completed telescope and spectrometer to develop the SOLARIS "blue" box. The HgCdTe detector is awaiting further quality control of its integration into its housing. The delay is a result of reduced funding and smaller size of the SOLARIS team, as the full CLARREO mission remains in extended pre-formulation. Delaying the HgCdTe integration has permitted the smaller SOLARIS team to continue testing of the calibration approaches and protocols with the "blue" spectrometer. Inclusion of the "red" spectrometer SOLARIS will eventually be required to demonstrate detector-based calibration approaches at longer wavelengths.

CLARREO RS Calibration & Characterization Approach The CLARREO Pathfinder RS spectrometer measurement and calibration approach is provided in Section 4.2. A critical part of the calibration is developing SI-traceable data by characterizing the sensor to SI-traceable, absolute radiometric quantities during prelaunch calibration to the electric Watt (prelaunch calibration box shown in Figure 4.3). Prelaunch absolute calibration includes both irradiance and radiance modes as well as the determination of geometric factors for conversion to reflectance. The end result of the prelaunch calibration is sufficient data to develop a sensor model that predicts the solar, lunar, and planetary/stellar sources planned for on-orbit calibration. Agreement between prelaunch and on-orbit values (as shown in Figure 4.3) implies the system is calibrated, and, by analogy, traceable to the pre-launch SI-traceable measurements. Disagreement implies that the sensor model requires improvement based on the on-orbit data, including an additional set of characterization measurements. Solar and lunar views provide information regarding temporal changes in the sensor once on-orbit traceability is established. Thus, the key to the RS on-orbit calibration is the prelaunch, SI-traceable calibration.

The required RS uncertainty is fully traceable to the electric Watt by applying tunable laser sources and detector-based standards. Calibration systems, such as NIST's Spectral Irradiance and Radiance Responsivity Calibrations using Uniform Sources (SIRCUS) facility, provide such standards and a capability to understand stray light, spectral response, and polarization sensitivity at the level necessary for CLARREO and CPF [*Brown et al.*, 2000]. The basis of SIRCUS is a well-understood tunable laser source that can be coupled to a fiber optic system providing both radiance and irradiance sources. The output of the source is determined via detector standards characterized against the Primary Optical Watt Radiometer (POWR). The planned calibration traceability to SIRCUS is shown as a stepwise sequence in Figure 4.6. It begins with a substitution radiometer that is used to calibrate

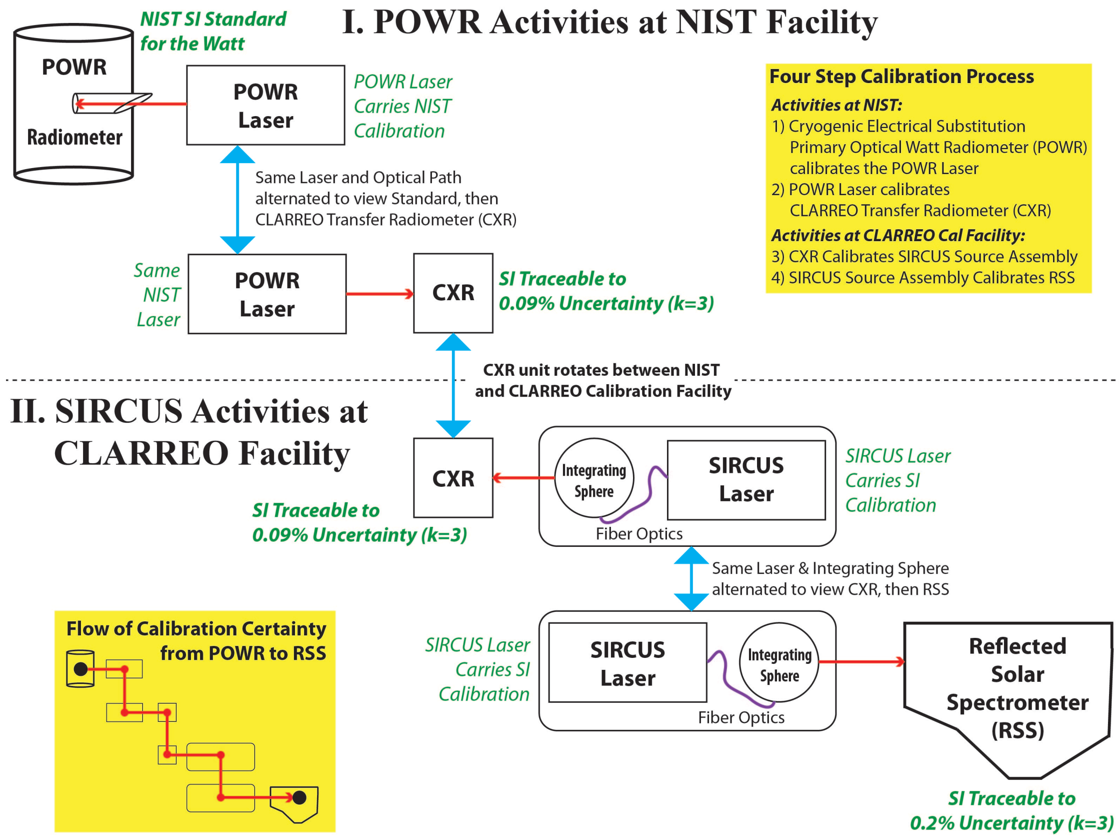

Figure 4.6: SIRCUS traceability of the CLARREO RS and SOLARIS calibration.

the tunable laser source, known as the POWR Laser. In a second step, the POWR unit is moved and replaced by the CLARREO Transfer Radiometer (CXR) based on a silicon-trap detector for the visible and near infrared and indium-gallium arsenide detectors at longer wavelengths. The stated accuracy to calibrate a transfer radiometer in irradiance mode using POWR is 0.09%($k = 3$). The upper portion of Figure 4.6 shows these steps.

The accuracy of such a radiance-based calibration has been demonstrated in NIST facilities to an expected accuracy of 0.2% for k=3. Once the CXR is calibrated, it is moved to the CLARREO Calibration Laboratory to calibrate the output of the sources used in the calibration of the RS instrument.

SOLARIS Test Plan The SOLARIS test plan evaluates all parts of the CLARREO/CPF calibration process, described in Section 4.2 and summarized in Figure 4.3, with emphasis on the laboratory-based absolute radiometric calibration. The SOLARIS test plan is shown in Figure 4.6. Attention is paid to developing credible uncertainties for characterizing possible degradation of the attenuator system. Emphasis of the laboratory testing is on the radiometric and spectral characterizations since the current state-of-the-art of geometric and spatial calibration approaches are sufficient for CLARREO mission requirements, assuming that stray light, scattered light, and ghosting analysis are radiometric properties. The importance of stray light in the reflectance retrieval makes characterization and modeling of stray and scattered light critical for SOLARIS, and the field-based measurements of the sun and surface reflectance retrievals essential to demonstrate understanding of the error budgets.

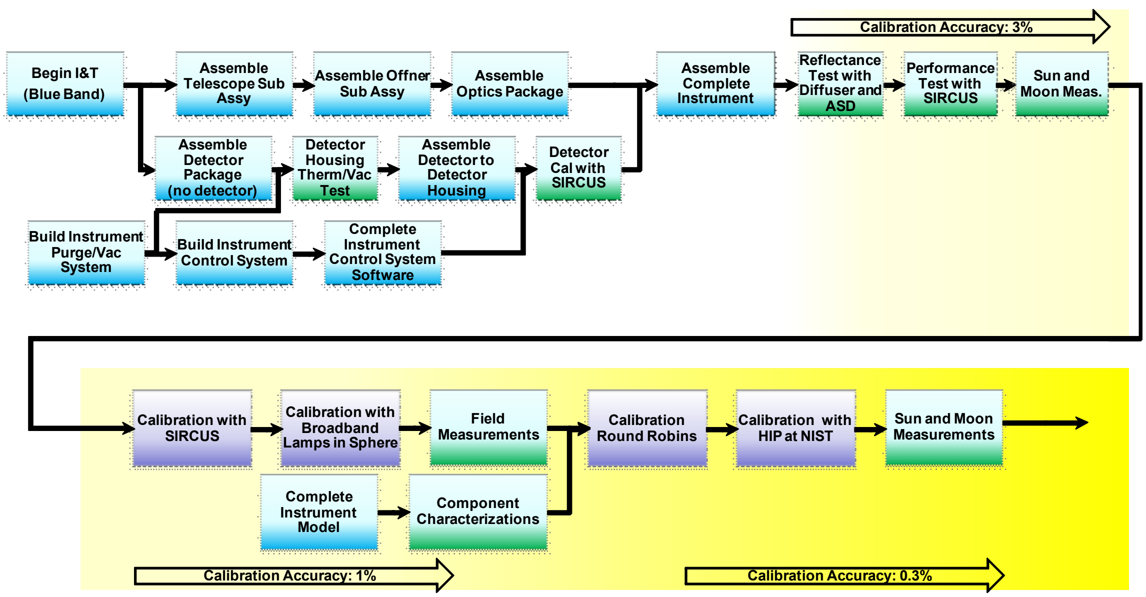

Figure 4.7: SOLARIS integration and test plan.

SOLARIS testing will lead to an end-to-end instrument performance model and error budgets with measured uncertainty magnitudes and peer reviewed measurement accuracy traceability chains, all of which are applicable to CLARREO/CPF. The path to an SI-traceable error budget leads to the CLARREO/CPF-required absolute uncertainties. Figure 4.7 shows the three phases of SOLARIS integration and testing that leads to the required level of accuracy:

1. 3% absolute uncertainty;
2. 1% absolute uncertainty; and
3. 0.3% absolute uncertainty.

Current budgetary restrictions result in limitations on the available calibration and sensor hardware such that the CDS goal is to demonstrate <1 % absolute uncertainty with a path to the full CLARREO mission requirement of 0.3% (k=2). SOLARIS will show these uncertainties for reflectance retrieval using direct solar irradiance to demonstrate SI-traceability of reflectance through both source- and detector-based standards.

The testing in each of the three phases is described below. All three phases follow the general philosophy to accomplish the following:

1. Develop and evaluate calibration protocols leading to an SI-traceable calibration of the SOLARIS;

2. Develop a physically-based spectrometer model;
3. Create a defensible error budget;
4. Implement a tunable laser facility with sufficient spectral coverage to cover the full CLARREO spectral range;
5. Evaluate broadband stray light;
6. Understand depolarizer technology;
7. Determine the impact of thermal control uncertainties of attenuators and detector;
8. Field collections with SOLARIS to provide a check on instrument models;
9. Inter-comparisons with other systems;
10. Characterization of solar and lunar irradiance; and
11. Retrieval of reflectance via direct solar view comparison.

While this list is strictly not in order of priority or importance, the first three items are considered to be the most important to the CLARREO project, and strictly speaking, ensure that the others occur.

Included in the Phase 1 was evaluation of SOLARIS hardware at the component and subsystem level prior to assembly of the sensor. The key components under consideration were the optical elements including the slit and grating, the detector package, and attenuation and depolarizer elements. The assembled instrument was used in the laboratory as part of preliminary detector-based calibrations [*Brown et al.*, 2000] and in the field with solar- and diffuser-based reflectance retrievals and lunar measurements to demonstrate the 3% absolute uncertainty. The error budget demonstrating the 3% level of uncertainty was evaluated in November 2013 as part of a CLARREO internal review that included the Science Definition Team and NIST evaluators. Phase 2 of the testing is achieving absolute uncertainties < 1 % (k = 2) by improving knowledge of the transfer radiometers that are part of the detector-based methodology. Additional component-level testing takes place to improve the knowledge of the instrument model leading to the 1% uncertainty error budget for the reflectance retrieval. Phase 3 concentrates on taking the uncertainties to the 0.3% level and concludes with an independent review of the error budget by NIST.

SOLARIS Initial Testing Results Initial testing of SOLARIS took place at the component and subsystem level prior to assembly of the sensor. The key components characterized were optical elements including the slit and grating, the detector package, and attenuation and depolarizer elements. Preliminary results of these tests are provided below. Also provided are early results from the laboratory testing of radiometric and spectral parameters, with concentration on the stray and scattered light characteristics needed to develop the optical model or to provide guidance for modifications to the SOLARIS optical system to limit these effects. The SOLARIS calibration demonstration is of the retrieved reflectance and as such must include field-based measurements of the sun and surface reflectance retrievals.

Lunar collections are also coupled with the field work to evaluate SOLARIS repeatability using the Moon.

Detector tests: Component-level testing of the detectors, both Silicon and HgCdTe, were used to select optimal wafers from multiple production runs that traded spectral response at shorter wavelengths against spectral coverage. Testing took place in the detector characterization laboratory at GSFC and included measurements of relative spectral response (RSR), detector-to-detector uniformity, noise, and temperature sensitivity. Physical measurements of pixel pitch and orientation of array relative to fiducials were also made. The next stage of detector evaluation occurred after assembly of the focal plane within the detector housing to protect the detector from contamination. Performance characterization followed with evaluation of RSR from 300 to 1200 nm to define the point at which detector response reaches the noise floor. Testing occurred with the housing at ambient temperature conditions with the detectors cooled to their operational levels. Testing was repeated in cold operational conditions. The data collected permitted evaluation of detector noise, dark current level and stability, relative spectral response, conversion efficiency (CE) level and stability, detector-to-detector uniformity, and linearity. Testing of the relative spectral response for the detectors was via a standard monochromator approach.

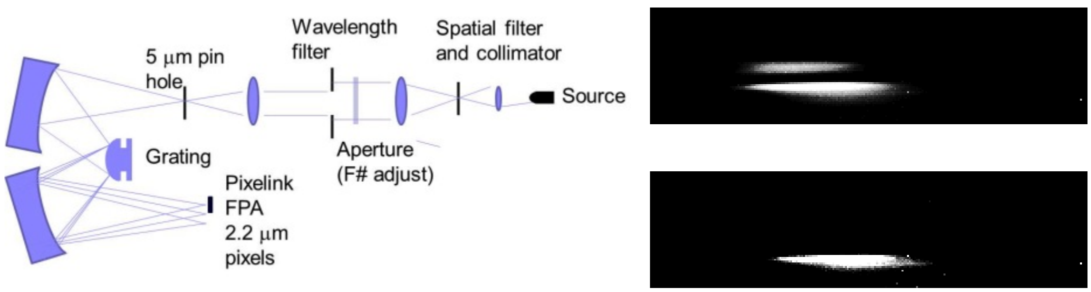

Figure 4.8: Test configuration for testing the optical and spectral quality of the blue spectrometer grating. Test results are shown on the right corresponding to pre- (upper) and post-baffling (lower) to eliminate a manufacturing artifact.

Grating Characterization: Grating characterization verified grating performance and its dimensional metrology. Dimensional metrology determined the size, shape, radius of curvature, and conic constant. The metrology also permitted assessing the optical quality of the grating through direct microscopic means. Optical characterization made use of the test configuration shown in Figure 4.8. Spectral evaluation made use of narrowband interference filters permitting determination of key spectrometer performance variables. Sample images from the high resolution imager at the end of the optical train are provided in Figure 4.8 as an example of the utility of these data. The horizontal and vertical size of the image provides the spatial and spectral quality of the grating. The top image demonstrates the effect of a manufacturing artifact that was observed during the direct metrology of the grating. Altering the positioning of the grating, proper baffling and slit design mitigated the impact of this artifact in the integrated system, as shown in the bottom image of Figure 4.8.

Optical Elements: The telescope and spectrometer optics were evaluated in like fashion to the grating. Dimensional metrology at the end of fabrication determined the size and shape of each element, including radius of curvature and conic constant. The metrology also evaluated the mechanical aspects of the elements and their associated mounts.

Performance characterization evaluates the quality of the surface finish and reflection efficiency as a function of wavelength. Surface figure of the optical elements was evaluated using standard optical interferometry techniques to evaluate wavefront error, and this was done under varying thermal conditions to understand the mirror's behavior with temperature.

Our results indicate the high-quality of the telescope elements. The relatively good agreement with the model indicates that the optical elements were properly aligned and the optical model is an adequate representation of the sensor.

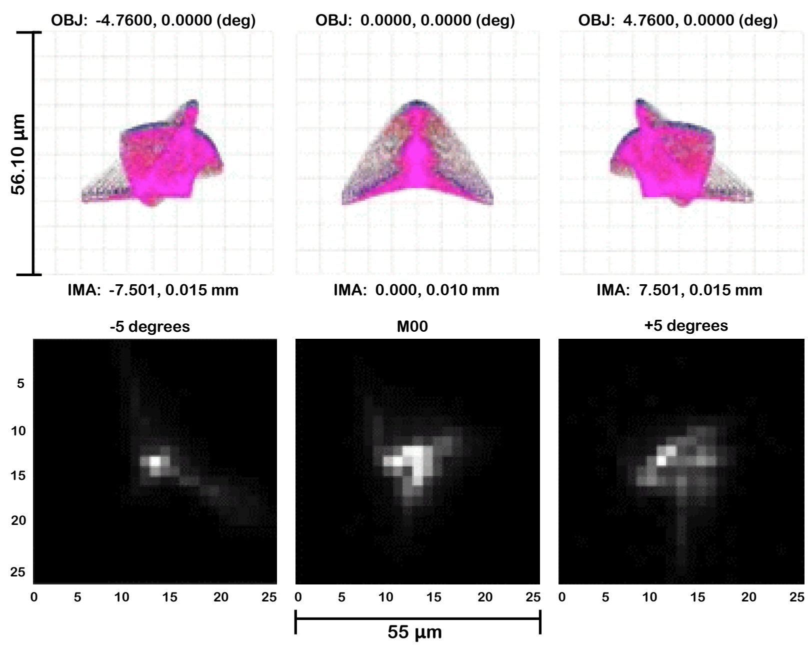

Figure 4.9: Top: modeled spot diagram results for SOLARIS telescope for sources at −5°, 0°, and +5°, and Bottom: measured camera output from a collimated source at the same angles illuminating the telescope.

Further comparison of the optical performance of SOLARIS relative to predictions from optical modeling is shown in Figure 4.9. The upper portion of the figure shows the spot diagrams for a point source located at −5°, 0°, and +5° from the optical axis. The lower portion of the figure shows imagery obtained by a high-spatial resolution camera placed behind the SOLARIS telescope and illuminated with a collimated source at the same angles as modeled. The imagery and model output are remarkably similar, save for slight rotational differences in the orientation of the patterns.

The spectral reflectance of the coatings of the mirrors was also measured to allow prediction of the sensor signal to noise. The spectral resolution of the reflectance measurements was sufficient to allow it to be combined with grating and detector response. Initial characterizations of the mirrors demonstrated that the coatings did not meet the required spectral reflectance at shorter wavelengths. The mirrors were recoated to ensure that the signal-to-noise would be sufficient in the ultraviolet while being as free as possible from spectral absorption features in the coating.

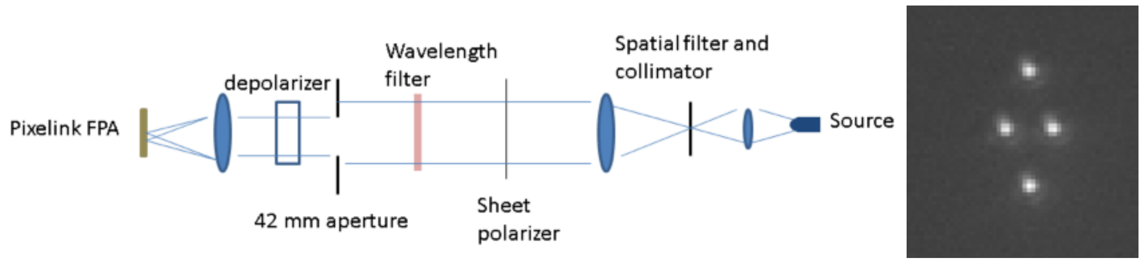

Figure 4.10: Schematic of experimental set up used to evaluate the performance of the SOLARIS depolarizers along with the image recorded by a commercially available, high resolution camera system of a collimated source. Each point is the result of the two wedges producing two polarization states. The ensemble of four points is smaller than the size of the SOLARIS pixel pitch.

Depolarizer: The quartz-quartz wedge depolarizer approach was selected for SOLARIS due to its compactness and its wide use in similar applications. Figure 4.10 shows a schematic of the experimental set up that was used to evaluate the performance of the SOLARIS depolarizers. The source in the figure consisted of a spherical integrating source coupled with a collimator that allowed $\pm 5°$ of tilt incidence at different f-stop numbers. A Moxtek wire-grid style broadband polarizer mounted within a rotation stage that allowed rotation through 360° acted as a reference calibration polarizer or "analyzer." The analyzer was incrementally rotated through 360° to characterize the degree of polarization of the light exiting the assembly. A set of narrow-band filters provided spectral selection.

The collimated source passed through the depolarizers to be imaged on a commercially available, high resolution camera system. The image shown on the right side of Figure 4.10 shows the results from a single analyzer position at a wavelength of 490 nm (through a 10-nm bandpass filter). The source was stopped down by a 5 μm pinhole. Each point in the image is the result of the two wedges producing two polarization states for a total of four points. The brightness of each point varies with the overall polarization of the source. The result matches analytical predictions with the left to right spot separation being 22 μm and the top to bottom spot separation being 60 μm. Collecting the light from all four points would ensure that integrated measurement is polarization insensitive. Ensuring that the size of the four-spot diamond fits within the SOLARIS detector would lead to a polarization-insensitive sensor.

Attenuators: The RS measurement requirement to obtain spectral reflectance relative to the solar irradiance drives the need to view the sun and requires attenuation of up to a factor of 1:50,000 relative to a typical Earth scene. The baseline design of the attenuator system includes a pinhole aperture, a perforated plate, and neutral density filters. The nominal size of the pinhole aperture would need to be 500 μm for the CLARREO application, but apertures of this size are associated with significant diffraction effects that vary strongly with wavelength. Characterization of the neutral density filters has followed standard approaches using monochromator measurements to determine the spectral transmittance.

The perforated plate is a grid of over 300 discrete pinholes attenuating through blockage and diffraction. A random hexagonal grid of pinholes with a random phase of 0.6 μm reduces artifacts from the system. The size of the perforated area and number of pinholes is designed to be large enough to produce a uniform beam across multiple detectors while avoiding edge effects. The pinhole density is uniform so that each detector in the focal plane sees the same number of pinholes. Randomizing the grid by varying pinholes prevents problems associated with the geometric regularity of mesh attenuators. Similarly, vignetting is avoided through both the random grid design and the operations concept of nominal 90° solar incidence angle.

Characterization of the pinholes to date has relied on measurements performed by the manufacturer as well as preliminary measurements with a laser-based system [*Brown et al.*, 2000]. Future measurements will include imaging approaches using electron microscopy or similar approaches to evaluate the shape, size, and total area of the pinholes.

Instrument-level laboratory testing: Instrument-level testing follows basic testing protocols for most passive, hyperspectral, imaging sensors. Collimated sources are used to evaluate spatial characteristics of the sensor and extended sources for the radiometric characterization. Inclusion of new sources is planned such as RF lamps to enhance blue light output [*Arecchi et al.*, 2011]. The approach to establish SI-traceability is to the standard Watt via NIST's POWR facility and through development of SIRCUS-like sources [*Brown et al.*, 2000].

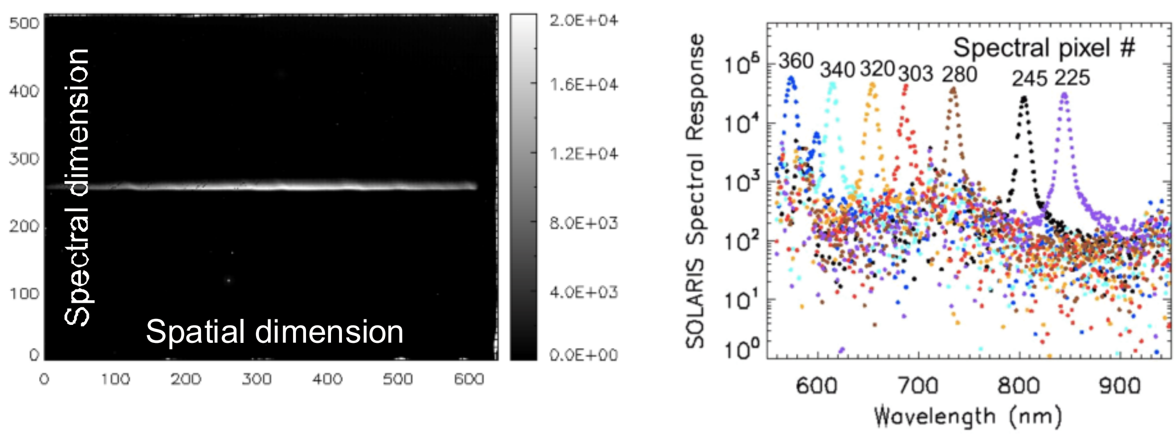

Figure 4.11: The SOLARIS output resulting from the illumination by a monochromatic, wide-field source (left image), and the results from several hundred such images to produce absolute spectral response of SOLARIS for seven representative bands (right image).

Absolute Radiometry Tests: The use of SIRCUS is the key to achieving calibration against both NIST standards and with respect to SI-traceable standards. The difficulty with a SIRCUS-based approach for absolute spectral response is the time-consuming nature of the measurements.

Figure 4.11 (left) shows the SOLARIS image from a single SIRCUS wavelength from a wide field spherical integrating source. The narrow vertical extent of the image is indicative of the near-monochromatic nature of the incident source. The wide spatial extent is the result of the wide field illumination. Each individual data point in Figure 4.11 (right) is the result of a single image as demonstrated in the left image. It should be noted that these data required several days to collect. The advantages of such data are the high accuracy of the absolute calibration, excellent knowledge of out-of-band response, and SI-traceability. The results shown in Figure 4.11 indicate that the spectrometer portion of SOLARIS is behaving as expected. There are no significant sources of out-of-band light except for higher order diffraction effects that can be corrected by appropriate filtering techniques. One key lesson learned to date from the SOLARIS absolute calibration collections is the need for improved lasers within the SIRCUS system to increase signal levels at the sensor, increase spectral coverage, and decrease the time needed to scan through the full spectrum under study.

The benefit of a nearly monochromic source is that collimating that source will provide a singular point on the imaging spectrometer's output. Figure 4.12 shows this singular point (labelled "Point source image" in the figure). Two other features are noticeable in the image as well. The lower feature is the result of higher-order diffraction effects in the grating and the fact that there is no filter in SOLARIS to remove this effect. The feature to the left of the point-source image is a result of an un-baffled reflection from the spectrometer's slit. The image shown in Figure 4.12 resulted in a modification to the SOLARIS optical train to add a baffle that removes this feature.

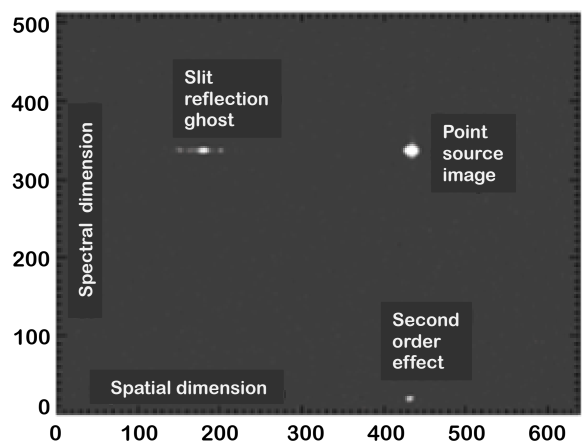

Figure 4.12: Image shows the SOLARIS output from a collimated, monochromatic source indicating a spatial stray light feature resulting from a reflection from the slit.

Relative Radiometry Tests: Parameters covered under the relative radiometry term include signal-to-noise ratio (SNR), noise characteristics, and detector-to-detector variability. These will make use of full-field, full-aperture sources and thus include all detectors in the evaluations. Thus, a portion of the relative radiometry process will be assessment of the temporal stability and spatial uniformity of the sources.

An initial evaluation of SOLARIS noise characteristics included data collected in three sweeps with 50 frames collected for exposure times varying from 5 to 900 ms. Collections at 5, 10, 15, 20, 25, and 30 ms were made at 10 frames per second, while those at 50, 100, 150, 200, and 250 ms were done at 3 frames per second. The last four exposure times of 300, 500, 700, and 900 ms included SOLARIS images at 1 frame per second.

Determining the dominant noise types is important for CLARREO because the climate record relies on averaging thousands of spatial data points over time to remove short-term reflectance variations in the Earth-atmosphere system. This allows the SNR requirement for CLARREO to be significantly lower than process-based missions, but requires that noise in the sensor be random. The low SNR of SOLARIS makes assessing the noise characteristics a challenge. Evaluation of the data relied on averages of all 50 frames per integration time as well as averages of sets of 10 frames. Mitigation of the relatively high noise of SOLARIS was accomplished by averaging 4×4 detectors. The ROIC used by SOLARIS relies on four separate amplifier chains, and the detectors were separated and evaluated by each amplifier chain.

The results indicate that the noise decreases by a factor of $5^{1/2}$ when comparing 10 frames versus 50 frames. This is as expected for a Gaussian- or shot-noise case and is the goal of the CLARREO design as it means that increased sampling will improve the overall signal-to-noise characteristics without creating a measurement bias. The averaging of the 16 spatial detectors did not, however, lead to a factor of four improvement in signal-to-noise. The result is still under evaluation since one possible cause would be a lack of independence between the 16 detectors being averaged as a result of a flaw in the focal plane electronics. A set of newer electronics that are closer to flight-like quality have recently been implemented, and its noise will be characterized in the future.

Sensor Linearity Tests: The fact that SOLARIS should have a highly non-linear sensor response, as a result of selecting a detector and electronics package that provides the dynamic range needed for a solar and Earth view approach, prompts for treating linearity as a specific item. Linearity characterization is done via three methods:

1. varying integration time;
2. varying source output via multiple apertures; and
3. varying source output via inclusion of attenuating filters.

The first approach is necessary to allow characterization of the 9803 ROIC behavior at low-light levels.

Evaluation of the noise characteristics, described above, was also used to determine sensor linearity. The approach is very similar to that developed for the Thermal Infrared Sensor (TIRS) on the Landsat 8 platform [*Montanaro et al.*, 2013], which uses an identical ROIC as in SOLARIS. The linearity correction developed for SOLARIS has been shown to be more accurate than that for TIRS, but is still at an error level too large for the CLARREO mission. Evaluations are currently underway to determine whether an alternate correction approach can reduce the errors or whether a different electronics design is needed for CLARREO.

Sensitivity to Polarization Tests: The same source and linear polarizer, as used to evaluate the depolarizer optics, is deployed at the instrument-level tests – the polarizer is rotated while recording the output of SOLARIS. The measurements are complicated by the fact that the polarized source must be known in a relative fashion to better than 0.5% to allow determination of the SOLARIS polarization sensitivity at levels required for CLARREO. Efforts to date have concentrated on understanding the polarization of the SIRCUS laser coupled to the spherical integrating source and the polarizer filter. Evaluations using a non-imaging field spectrometer, the SOLARIS sensor, and the transfer radiometers used to calibrate the SIRCUS output indicate that the sphere source is depolarized to better than the 0.5% level. While such results would typically lead to the conclusion that the source is effectively unpolarized, the strict requirements for SOLARIS means that further evaluation of the polarization test set up is needed.

Instrument-level Field Testing: The baseline approach to on-orbit radiance knowledge is that the Sun provides a reliable source for transfer to orbit and for maintaining calibration on-orbit. The goal of field measurements is to develop the techniques needed to ensure an accurate transfer to orbit while at the same time demonstrating that a direct solar view can be used to determine surface reflectance. Lunar data are to be collected to verify the calibration of the attenuators.

Demonstration of SOLARIS in the field took place in early 2012 with measurements of an Earth scene converted to reflectance via inclusion of a reflectance standard in the image. Analyses of these data pointed to several issues related to portability, sensor frame rate, and stray light features. This led to the implementation of a field portable version called Suitcase SOLARIS. The design made use of an additional set of optics, grating, and housing coupled to an off-the-shelf silicon charge-coupled device (CCD) array package. This system is not intended to retrieve solar-Earth view ratios, thus can rely on detector packages with smaller well depths. The data from Suitcase SOLARIS rely on the laboratory radiance calibration before and after deployment.

The Suitcase SOLARIS was completed in March 2013 and deployed in April 2013 in the southwest deserts in Arizona, California, and Nevada as part of early on-orbit evaluation of the Landsat-8 Operational Land Imager. The goal of the deployment was to evaluate intercalibration approaches proposed for CLARREO, and included ground-based measurements of surface-leaving radiance by Suitcase SOLARIS timed to coincide with overpasses of Landsat-7, Landsat-8, and an airborne imaging spectrometer. The data set will provide an ability to test the robustness of the SOLARIS design as well as traceability protocols since all of the sensors used during the field measurements can be traced to the SIRCUS-like calibration approach.

4.3.3 Reflected Solar Prototype Instrument Development at CU-LASP

The HyperSpectral Imager for Climate Science (HySICS), developed by Greg Kopp and the team at the University of Colorado's Laboratory for Atmospheric and Space Physics (LASP), is a testbed demonstrating improved techniques for future space-based radiance studies, and results from the ESTO-funded IIP projects from 2007 and 2010. The calibration method developed by the HySICS team improves the SI-traceable accuracy by a factor of $\sim$10 to the required levels for the CLARREO Scientific Objective of measuring the solar radiation reflected by the Earth. This hyperspectral imager will trace its calibration on orbit through the solar spectral irradiance recommended in the Decadal Survey [*National Research Council*, 2007]. Solar irradiance is known to better radiometric accuracy than any other calibration source available on orbit. By cross-calibrating a hyperspectral imager with solar spectral irradiance, using techniques LASP has proven on other spaceflight instruments, the Earth-viewing imager can be calibrated, validated, and tracked on orbit to the required accuracy and traceability levels. A polarization insensitive design, plus polarimetry capabilities, help achieve CLARREO radiometric accuracies needed for climate benchmarking and cross-calibration.

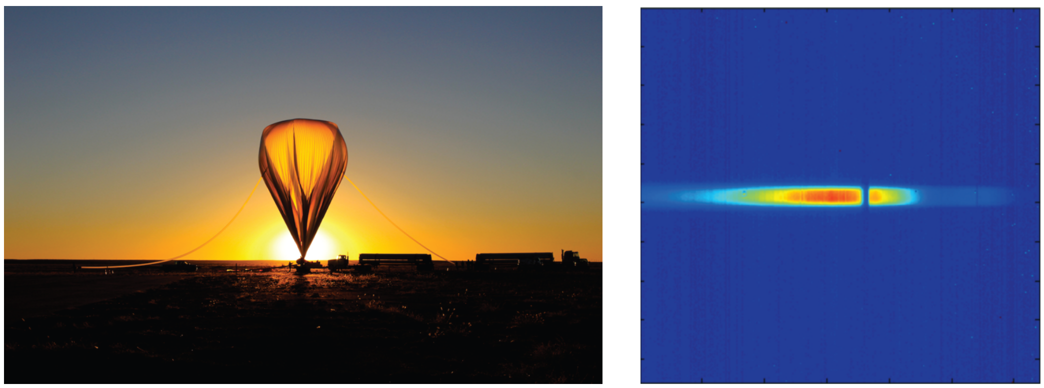

Figure 4.13: From the HySICS demonstration on September 29, 2013. Left: The high-altitude balloon that carried the HySICS instrument to the outermost part of Earth's atmosphere was inflated with helium. Right: The spatial-spectral scans of the sun enable HySICS's accurate radiometric calibrations.

In September 2013, HySICS made its inaugural engineering flight on a high-altitude balloon from Fort Sumner, NM (Figure 4.13). Balloon flights provide realistic, space-like conditions at a fraction of the cost of launching an instrument into space, and are therefore an ideal means of testing new space-based technologies. From a height above most of Earth's atmosphere of 125,000 feet (38 km), HySICS, aided by the pointing precision of the NASA Wallops Arc Second Pointer (WASP), was able to make measurements of the Earth, sun, and moon during both daylight and night hours. The instrument performed as expected on the eight and a half hour flight, collecting radiance data and periodically calibrating itself with highly accurate radiance scans of the sun (Figure 4.13) and moon. The data collected during the engineering flight will be used to improve the instrument over the next year and to further advance the science algorithms used to process the data. HySICS images scenes onto a single focal plane array at wavelengths between 350 and 2300 nm, covering the extremely important solar and near infrared spectrum containing most of the sun's emitted energy. Using only a single array allows HySICS to be smaller and lighter than many imagers, a feature necessary for cost-effective space-based Earth observing missions.

The precision pointing that is critical to calibrations using HySICS' three different targets – the Earth, sun, and moon – during one short flight was made possible by WASP, a balloon-based tool originally developed for planetary scientists to aim their instruments at distant items of interest. WASP, developed at the NASA Wallops Flight Facility in Virginia, took its first balloon test flight in 2011 and another engineering flight in 2012. After extensive testing, WASP was partnered with its first science instrument, HySICS, for the radiance instrument's inaugural engineering flight.

A second balloon flight was made in September 2014. After a successful mid-morning liftoff and reaching an altitude high enough to provide the imager with nearly a 7-kilometer field-of-view of the ground, HySICS collected science data and self-calibrated by periodically taking radiance measurements of the sun and moon. The calibration against the sun's known emitted energy provides the instrument with a reference point that allows it to collect highly accurate data of the Earth.

From liftoff to landing, HySICS and WASP were airborne for nearly nine hours. When the team had collected enough data to test the accuracy of the instrument, the balloon payload was separated from the balloon itself and was safely carried back to the ground via parachutes, landing between two threatening thunderstorms. The payload landed east of Holbrook, Arizona. The flight was deemed both an operational and scientific success. The HySICS team was able to collect high-quality radiance measurements throughout the flight and has processed and analyzed the on-board data.

4.3.4 NIST Calibration Activities for CPF

In Section 4.3.1, the NIST activities in support of the NASA CLARREO mission between 2010 and 2014 are summarized. During the first two years, NIST's activities were fairly evenly divided between the CLARREO RS and IR instruments, multiple ideas for collaboration between NIST and NASA were proposed, and some were pursued. In the CLARREO extended pre-formulation phase that began in 2011, the NIST tasks were more tightly directed toward the RS and IR Calibration Demonstration Systems (CDS). Here, the RS spectrometer-supported NIST activities will be further discussed.

The primary technical activities between NASA GSFC and NIST were centered around the use of the NIST Spectral Irradiance and Radiance Calibrations with Uniform Sources (SIRCUS) technique for pre-flight RS calibration. In this technique, the flight instrument views the radiance from an integrating sphere that is illuminated by a tunable laser. The laser can be tuned across the RS instrument spectral range, and the radiance calibrated by a NIST-calibrated detector substituted in the position of the RS instrument. This technique has been viewed from the outset as a promising method for characterizing the RS instrument for stray light and perhaps for ultimately calibrating the RS instrument. To facilitate its use for CLARREO, and ultimately CPF, NIST procured a portable version of the SIRCUS hardware and provided it to NASA Goddard on long-term loan. NIST staff also trained NASA Goddard staff on the operation of the SIRCUS instrument at Goddard, assisted NASA with the specifications for procurement of the reference detectors, and calibrated the reference detectors.

Additional (NIST-funded) activities at NIST related to the RS instrument included development of an absolute detector-based source (ADbS) and the Hyperspectral Image Projector (HIP). Each of these uses a spectral light engine to provide broadband, programmable spectra. The output of the ADbS is calibrated using a broadband detector by tuning each monochromatic spectral channel individually. The ADbS developments used a commercially-available lamp-based spectral light engine. Two papers were written on the ADbS (2010 SPIE and a manuscript headed for J. Res. NIST). The HIP uses a commercially-available supercontinuum source and is otherwise a custom instrument. It presents realistic spatial and spectra scenes to the sensor being tested many SPIE papers were written on the HIP. The HIP prototype was used in 2011 with a CLARREO-relevant hyperspectral imager prototype developed by the University of Colorado Laboratory of Atmospheric and Space Physics (LASP) under an NASA IIP project to provide an initial test of the concept. A hyperspectral image was projected by the HIP into the LASP sensor and measured at the end of a two-week visit of the LASP sensor to the NIST HIP facility.

5 References

Arecchi, A. V., G. A. McKee, and C. N. Durell (2011), Rf-excited plasma lamps for use as sources in ogse integrating spheres, in *SPIE Optical Engineering+ Applications*, pp. 81,530W–81,530W, International Society for Optics and Photonics.

Bony, S., R. Colman, V. M. Kattsov, R. P. Allan, C. S. Bretherton, J.-L. Dufresne, A. Hall, S. Hallegatte, M. M. Holland, W. Ingram, et al. (2006), How well do we understand and evaluate climate change feedback processes?, *Journal of Climate*, *19*(15), 3445–3482.

Bovensmann, H., J. Burrows, M. Buchwitz, J. Frerick, S. Noël, V. Rozanov, K. Chance, and A. Goede (1999), Sciamachy: Mission objectives and measurement modes, *Journal of the Atmospheric Sciences*, *56*(2), 127–150.

Brown, S. W., G. P. Eppeldauer, and K. R. Lykke (2000), Nist facility for spectral irradiance and radiance responsivity calibrations with uniform sources, *Metrologia*, *37*(5), 579.

Brown, S. W., G. P. Eppeldauer, and K. R. Lykke (2006), Facility for spectral irradiance and radiance responsivity calibrations using uniform sources, *Applied Optics*, *45*(32), 8218–8237.

Cox, C., and W. Munk (1956), Slopes of the sea surface deduced from photographs of sun glitter, *Scripps Institution of Oceanography.*

Eplee, R. E., G. Meister, F. S. Patt, R. A. Barnes, S. W. Bailey, B. A. Franz, and C. R. McClain (2012), On-orbit calibration of seawifs, *Applied optics*, *51*(36), 8702–8730.

Espejo, J., G. Drake, K. Heuerman, G. Kopp, A. Lieber, P. Smith, and B. Vermeer (2011), A hyperspectral imager for high radiometric accuracy earth climate studies, in *SPIE Optical Engineering+ Applications*, pp. 81,580B–81,580B, International Society for Optics and Photonics.

Evans, K., and G. Stephens (1991), A new polarized atmospheric radiative transfer model, *Journal of Quantitative Spectroscopy and Radiative Transfer*, *46*(5), 413–423.

Fox, N., A. Kaiser-Weiss, W. Schmutz, K. Thome, D. Young, B. Wielicki, R. Winkler, and E. Woolliams (2011), Accurate radiometry from space: an essential tool for climate studies, *Philosophical Transactions of the Royal Society of London A: Mathematical, Physical and Engineering Sciences*, *369*(1953), 4028–4063.

GCOS-154 (2011), Systematic observation requirements for satellite-based data products for climate, 2011 update, *Tech. rep.*, World Meteorological Organization.

Goldberg, M. D. (2007), Global space-based inter-calibration system (gsics), in *Optical Engineering+ Applications*, pp. 668,402–668,402, International Society for Optics and Photonics.

Hansen, J., and J. Hovenier (1971), The doubling method applied to multiple scattering of polarized light, *Journal of Quantitative Spectroscopy and Radiative Transfer*, *11*(6), 809–812.

Kieffer, H. H. (1997), Photometric stability of the lunar surface, *Icarus*, *130*(2), 323–327.

Kieffer, H. H., and T. C. Stone (2005), The spectral irradiance of the moon, *The Astronomical Journal*, *129*(6), 2887.

Lacis, A., J. Chowdhary, B. Cairns, and M. Mishchenko (1998), Modeling errors in diffuse-sky radiation, *Geophys. Res. Lett*, *25*, 135–138.

Lautenbacher Jr, C. C. (2005), The global earth observation system of systems (geoss), in *Local to Global Data Interoperability-Challenges and Technologies, 2005*, pp. 47–50, IEEE.

Leroy, S. S., J. G. Anderson, and G. Ohring (2008), Climate signal detection times and constraints on climate benchmark accuracy requirements, *Journal of Climate*, *21*(4), 841–846.

Loeb, N. G., B. A. Wielicki, W. Su, K. Loukachine, W. Sun, T. Wong, K. J. Priestley, G. Matthews, W. F. Miller, and R. Davies (2007), Multi-instrument comparison of top-of-atmosphere reflected solar radiation, *Journal of climate*, *20*(3), 575–591.

Loeb, N. G., B. A. Wielicki, T. Wong, and P. A. Parker (2009), Impact of data gaps on satellite broadband radiation records, *Journal of Geophysical Research: Atmospheres*, *114*(D11).

Lukashin, C., B. A. Wielicki, D. F. Young, K. Thome, Z. Jin, and W. Sun (2013), Uncertainty estimates for imager reference inter-calibration with clarreo reflected solar spectrometer, *Geoscience and Remote Sensing, IEEE Transactions on*, *51*(3), 1425–1436.

Lukashin, C., Z. Jin, G. Kopp, D. G. MacDonnell, and K. Thome (2015), Clarreo reflected solar spectrometer: Restrictions for instrument sensitivity to polarization, *Geoscience and Remote Sensing, IEEE Transactions on*, *53*(12), 6703–6709.

Lyapustin, A., Y. Wang, X. Xiong, G. Meister, S. Platnick, R. Levy, B. Franz, S. Korkin, T. Hilker, J. Tucker, F. Hall, P. Sellers, A. Wu, and A. Angal (2014), Scientific impact of modis c5 calibration degradation and c6+ improvements, *Atmospheric Measurement Techniques*, *7*(12), 4353–4365, doi:10.5194/amt-7-4353-2014.

Masson, D., and R. Knutti (2011), Spatial-scale dependence of climate model performance in the cmip3 ensemble, *Journal of Climate*, *24*(11), 2680–2692.

Montanaro, M., Z. Tesfaye, A. Lunsford, B. Wenny, D. Reuter, B. Markham, R. Smith, and K. Thome (2013), Preliminary on-orbit performance of the thermal infrared sensor (tirs) on board landsat 8, in *SPIE Optical Engineering+ Applications*, pp. 88,661D–88,661D, International Society for Optics and Photonics.

Nadal, F., and F.-M. Bréon (1999), Parameterization of surface polarized reflectance derived from polder spaceborne measurements, *Geoscience and Remote Sensing, IEEE Transactions on*, *37*(3), 1709–1718.

National Research Council (2007), *Earth Science and Applications from Space: National Imperatives for the Next Decade and Beyond*, 428 pp., National Academy Press.

Ohring, G., B. Wielicki, R. Spencer, B. Emery, and R. Datla (2005), Satellite instrument calibration for measuring global climate change: Report of a workshop., *Bulletin of the American Meteorological Society*, *86*(9).

Ohring, G., J. Tansock, W. Emery, J. Butler, L. Flynn, F. Weng, K. S. Germain, B. Wielicki, C. Cao, M. Goldberg, et al. (2007), Achieving satellite instrument calibration for climate change, *EOS, Transactions American Geophysical Union*, *88*(11), 136–136.

Ramanathan, V., R. Cess, E. Harrison, P. Minnis, B. Barkstrom, E. Ahmad, and D. Hartmann (1989), Cloud-radiative forcing and climate: Results from the earth radiation budget experiment, *Science*, *243*(4887), 57–63.

Richard, E., D. Harber, J. Rutkowski, K. O?Malia, M. Triplett, G. Drake, J. Harder, P. Pilewskie, S. Brown, A. Smith, et al. (2011), Future long-term measurements of solar spectral irradiance by the tsis spectral irradiance monitor: Improvements in measurement accuracy and stability, in *Proceedings 11th International Conference on New Developments and Applications in Optical Radiometry*, paper INV004.

Roe, G. H., and M. B. Baker (2007), Why is climate sensitivity so unpredictable?, *Science*, *318*(5850), 629–632.

Roithmayr, C., C. Lukashin, P. Speth, D. Young, B. Wielicki, K. Thome, and G. Kopp (2014), Opportunities to intercalibrate radiometric sensors from international space station, *Journal of Atmospheric and Oceanic Technology*, *31*(4), 890–902.

Roithmayr, C. M., and P. W. Speth (2012), Analysis of opportunities for intercalibration between two spacecraft, *Advances in Engineering Research*, *1*, 409–436.

Soden, B. J., and I. M. Held (2006), An assessment of climate feedbacks in coupled ocean-atmosphere models, *Journal of Climate*, *19*(14), 3354–3360.

Soden, B. J., I. M. Held, R. Colman, K. M. Shell, J. T. Kiehl, and C. A. Shields (2008), Quantifying climate feedbacks using radiative kernels, *Journal of Climate*, *21*(14), 3504–3520.

Stamnes, K., S.-C. Tsay, W. Wiscombe, and K. Jayaweera (1988), Numerically stable algorithm for discrete-ordinate-method radiative transfer in multiple scattering and emitting layered media, *Applied optics*, *27*(12), 2502–2509.

Stocker, T. F., D. Qin, G.-K. Plattner, M. Tignor, S. K. Allen, J. Boschung, A. Nauels, Y. Xia, V. Bex, and P. M. Midgley (2013), Climate change 2013: The physical science basis, *Intergovernmental Panel on Climate Change, Working Group I Contribution to the IPCC Fifth Assessment Report (AR5)(Cambridge Univ Press, New York)*.

Stott, P. A., and J. Kettleborough (2002), Origins and estimates of uncertainty in predictions of twenty-first century temperature rise, *Nature*, *416*(6882), 723–726.

Sun, J.-Q., and X. Xiong (2007), Modis polarization-sensitivity analysis, *Geoscience and Remote Sensing, IEEE Transactions on*, *45*(9), 2875–2885.

Sun, W., and C. Lukashin (2013), Modeling polarized solar radiation from the ocean–atmosphere system for clarreo inter-calibration applications, *Atmospheric Chemistry and Physics*, *13*(20), 10,303–10,324.

Sun, W., G. Videen, and M. I. Mishchenko (2014), Detecting super-thin clouds with polarized sunlight, *Geophysical Research Letters*, *41*(2), 688–693.

Sun, W., C. Lukashin, R. R. Baize, and D. Goldin (2015a), Modeling polarized solar radiation for clarreo inter-calibration applications: Validation with parasol data, *Journal of Quantitative Spectroscopy and Radiative Transfer*, *150*, 121–133.

Sun, W., R. R. Baize, C. Lukashin, and Y. Hu (2015b), Deriving polarization properties of desert-reflected solar spectra with parasol data, *Atmospheric Chemistry and Physics*, *15*(13), 7725–7734.

Tanré, D., F. Bréon, J. Deuzé, O. Dubovik, F. Ducos, P. François, P. Goloub, M. Herman, A. Lifermann, and F. Waquet (2011), Remote sensing of aerosols by using polarized, directional and spectral measurements within the a-train: the parasol mission, *Atmospheric Measurement Techniques*, *4*(7), 1383–1395.

Von Storch, H., and F. W. Zwiers (2001), *Statistical analysis in climate research*, Cambridge university press.

Weatherhead, E. C., G. C. Reinsel, G. C. Tiao, X.-L. Meng, D. Choi, W.-K. Cheang, T. Keller, J. DeLuisi, D. J. Wuebbles, J. B. Kerr, et al. (1998), Factors affecting the detection of trends: Statistical considerations and applications to environmental data, *Journal of Geophysical Research: Atmospheres (1984–2012)*, *103*(D14), 17,149–17,161.

Wielicki, B. A., D. R. Doelling, D. F. Young, N. G. Loeb, D. P. Garber, and D. G. MacDonnell (2008), Climate quality broadband and narrowband solar reflected radiance calibration between sensors in orbit, in *Geoscience and Remote Sensing Symposium, 2008. IGARSS 2008. IEEE International*, vol. 1, pp. I–257, IEEE.

Wielicki, B. A., D. F. Young, M. G. Mlynczak, K. J. Thome, S. Leroy, J. Corliss, J. G. Anderson, C. Ao, R. Bantges, F. Best, K. Bowman, H. Brindley, W. Collins, J. A. Dykema, D. R. Doelling, D. R. Feldman, N. Fox, X. Huang, R. Holz, Y. Huang, Z. Jin, D. Jennings, D. G. Johnson, K. Jucks, S. Kato, R. Knuteson, G. Kopp, D. P. Kratz, X. Liu, C. Lukashin, A. J. Mannucci, N. Phojanamongkolkij, P. Pilewskie, S. Platnick, V. Ramaswamy, H. Revercomb, J. Rice, Y. Roberts, C. M. Roithmayr, F. Rose, S. Sandford, E. L. Shirley, S. W.L. Smith, B. Soden, P. W. Speth, L. Strow, W. Sun, P. Taylor, D. Tobin, and X. Xiong (2013), Achieving climate change absolute accuracy in orbit, *B. Am. Meteorol. Soc.*

Wu, A., X. Xiong, Z. Jin, C. Lukashin, B. N. Wenny, and J. J. Butler (2015), Sensitivity of intercalibration uncertainty of the clarreo reflected solar spectrometer features, *Geoscience and Remote Sensing, IEEE Transactions on*, *53*(9), 4741–4751.

A Appendix: Climate Trend Uncertainty

The accuracy of climate trends relative to a perfect climate observing system can be determined following a simple extension of the methodology of *Leroy et al.* [2008]. In particular, we can define a climate trend uncertainty factor, U_a, as the ratio of the accuracy of an actual observing system like CLARREO to that of a perfect observing system. This uncertainty factor is given by $U_a = (\delta m/\delta m_p)$, where δm is the accuracy of a climate trend with the CLARREO observations, and δm_p is the accuracy of the same climate trend for a perfect observing system. From *Leroy et al.* [2008] we can show that

$$(\delta m_p)^2 = 12(\Delta t)^{-3}(\sigma_{var}^2 \tau_{var}) \; , \tag{A.1}$$

and

$$(\delta m)^2 = 12(\Delta t)^{-3}(\sigma_{var}^2 \tau_{var} + \sum \sigma_i^2 \tau_i) \; . \tag{A.2}$$

Using Equations A.1 and A.2 the definition of the U_a, we can show that

$$U_a = (1 + \sum f_i^2)^{1/2} \; , \tag{A.3}$$

where

$$f_i^2 = \frac{\sigma_i^2 \tau_i}{\sigma_{var}^2 \tau_{var}} \; . \tag{A.4}$$

In Equations A.1 - A.4, σ_{var}^2 is the variance of the natural variability of the climate system for the variable of interest (SW CRF, spectral nadir reflectance, cloud cover, etc.); τ_{var} is the autocorrelation time for natural variability [*Leroy et al.*, 2008]; σ_i^2 and τ_i are the same two quantities for the variance and time-scale of observation error source, respectively; and Δt is the length of the climate time series. The units of the trend uncertainty provided by Equations A.1 and A.2 are defined by the units used in σ_{var}, τ_{var} and Δt. For example, use of the values from Table 2 will provide a trend uncertainty in temperature per year.

The autocorrelation time is a measure of the time between independent samples in a time series of measurements. The number of independent samples, in turn, governs the uncertainty due to noise in the measurement. Therefore, longer time scale error sources have a larger impact on uncertainty than shorter time scales. A key error source for decadal change is calibration accuracy, and its time scale is taken as the instrument lifetime on orbit [*Leroy et al.*, 2008]. The reason for this choice is that accuracy of an instrument can vary over time, while systematic errors are also likely to be present that are intrinsic to the instrument design itself and its limitations. As a result, for climate change we must consider the worst possible case that provides a calibration time scale of the life of the instrument, taken here as 60 months for CLARREO. For natural variability, the value of τ can be derived as in *Leroy et al.* [2008] or as in *Weatherhead et al.* [1998] (used in this study), where is τ is given by $\tau = (1+\rho)/(1-\rho)$, and where ρ is the lag-1 autocorrelation. For this study, we compared both methods and found similar results to within about 20%.

Finally, we can define an uncertainty factor, U_t, for climate trend detection. This uncertainty factor is the ratio of the time to detect climate trends at any confidence level for the CLARREO observing system to that of a perfect observing system. The result also can be derived from *Leroy et al.* [2008] using analogous definitions to Equations A.1 - A.4, and is given by

$$U_t = (1 + \sum f_i^2)^{1/3} \, . \tag{A.5}$$

Equations A.1 - A.5 provide a powerful method to understand the trade space of climate trend accuracy, detection, and observing system uncertainties.

B Appendix: Polarization Distribution Models

Reflected solar radiation from the Earth's ocean-atmosphere system (320 nm to 2300 nm wavelength range) can be significantly polarized by the Earth's surface and by atmospheric components. Effects from polarization of reflected light bias radiometric performance of various operational spaceborne instruments, such as MODIS and VIIRS, and imagers in geostationary orbits. It is essential to evaluate and correct for this bias in order to perform accurate measurements of reflectance at the top-of-atmosphere [*Lyapustin et al.*, 2014]. CLARREO's goal is to perform on-orbit inter-calibration with the target instrument by providing observations coincident in time and matched in space and viewing geometry. The inter-calibration process consists of iterative adjustments to the target sensor calibration to account for the polarization effects with respect to the observations made by CLARREO [*Lukashin et al.*, 2013]. Knowing the inter-calibrated instrument's on-orbit sensitivity to polarization and polarization state of reflected light would determine the radiometric polarization correction.

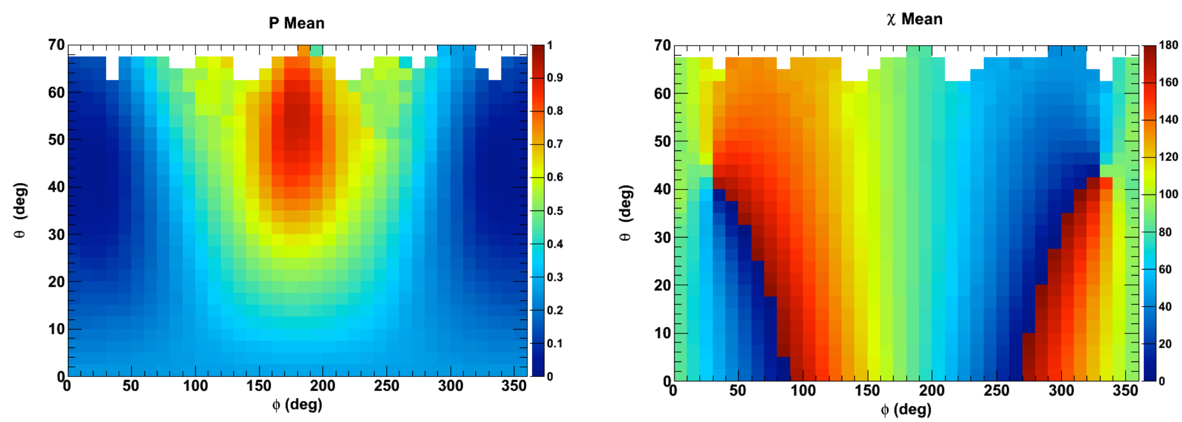

Figure B.1: PDM for the clear sky ocean scene based on PARASOL data. Left: degree of linear polarization, P. Right: angle of linear polarization, χ. Both parameters are averaged over the 2006 observations, for solar zenith angle between 40° and 50°, and plotted versus the viewing zenith angle (θ) and relative solar azimuth (ϕ).

A. Empirical Polarization Distribution Models

Feasibility of the on-orbit inter-calibration has been demonstrated using existing data – by developing the Polarization Distribution Models (PDMs) as functions of viewing scene type and geometry [*Lukashin et al.*, 2013, *Nadal and Bréon*, 1999]. A state of light at the top of the atmosphere is fully specified by three parameters: total radiance, I, degree of linear polarization, P, and angle of linear polarization, χ. Constructing a PDM is providing mean values and uncertainties for P and χ for every scene type globally, and as a function of solar and viewed geometry.

The only available dataset containing the polarization parameters measured on orbit was collected by the POLarization and Directionality of the Earth's Reflectances (POLDER) instrument onboard the Polarization and Anisotropy of Reflectances for Atmospheric Sciences coupled with Observations from a Lidar (PARASOL) satellite. The satellite was operational between 2004 and 2013 and was flying as part of the A-Train formation at 705 km altitude. The instrument consisted of a high-resolution CCD detector capable of taking measurements from nine spectral channels from blue (443 nm) to infrared (1020 nm), three of which, 490, 670, and 865 nm, measured polarization. A unique feature of the instrument was the multi-angular sampling of the same ground-pixel being imaged up to 15 times by the same pixel at different viewing angles.

From the Stokes parameters I, Q, and U measured by PARASOL, the relative degree of polarization P and the angle of linear polarization χ may be easily computed:

$$P = \frac{I_p}{I} = \frac{\sqrt{Q^2 + U^2}}{I}, \tag{B.1}$$

$$\chi = \begin{cases} \frac{1}{2}\text{arctan}(U/Q) \text{ for } Q > 0, U > 0 \\ \frac{1}{2}\text{arctan}(U/Q) + \pi \text{ for } Q > 0, U < 0 \\ \frac{1}{2}\text{arctan}(U/Q) + \pi/2 \text{ for } Q < 0 \end{cases} \tag{B.2}$$

where χ is defined from 0° to 180° relative to instrument viewing plane. A PDM for a given scene type and solar zenith angle can be represented by two-dimensional histograms of viewing zenith angle θ versus relative azimuth ϕ, with the color axis representing P or χ. An example of a PDM using the 2006 PARASOL dataset for the clear-sky ocean scene is shown in Figure B.1. The plots show the values of P and χ averaged over the entire year. We note that for these plots the solar zenith angle was restricted to values between 40° and 50° and wind speed to below 2.5 ms^{-1}. To ensure the purity of the clear-sky selection, cloud fraction was required to be less than 1%. Due to the near absence of aerosols, both P and χ exhibit nearly perfect forward/backward ($\phi < 180°/\phi > 180°$) scattering symmetry as expected. The maximum degree of polarization, 0.9, is found at $\phi = 180°$, the direction opposite the sun. That the degree of polarization is so high, close to its upper limit of 1, is not surprising given the highly polarizing nature of water surfaces. On the other hand, the degree of polarization is minimum when facing the sun and in Figure B.1 (left plot) is seen to be less than 0.1. An example of PDM distribution for polarization angle χ is shown in Figure B.1 (right plot). As expected, χ values are close to 90° in scattering plane ($\phi = 0°; 180°$).

The uncertainty on the reflectance measured by an imager, such as MODIS or VIIRS, after its inter-calibration with CLARREO may be found as:

$$\delta_{RI} = \sqrt{\delta_{\rho_0}^2 + \left(\frac{mP}{1 + mP}\right)^2 (\delta_m^2 + \delta_P^2)}\ , \tag{B.3}$$

where ρ_0 is the imager reflectance before the polarization inter-calibration is applied, m is the imager's sensitivity to polarization, and δ_{ρ_0}, δ_m and δ_P are the relative uncertainties on ρ_0, m and P, respectively. The δ_{ρ_0} in Equation B.3 is comprised of three components: CLARREO's own instrument accuracy (0.15%), inter-calibration sampling uncertainty after averaging (0.1%) and the target sensor stability uncertainty (0.1%). The combined value of the three uncertainties is 0.2%. The value of m is 0.03, which is roughly the sensitivity to polarization for both MODIS and VIIRS. Under these conditions, and using the P PDMs discussed above, we obtain the δ_{RI} dependencies as shown in Figure B.2. One finds that for realistic values of the uncertainty on the imager sensitivity, between 10% and 20%, the polarization bias can as high as nearly 1%. This dependency can be shown to be nearly invariant for bands between 670 nm and 865 nm.

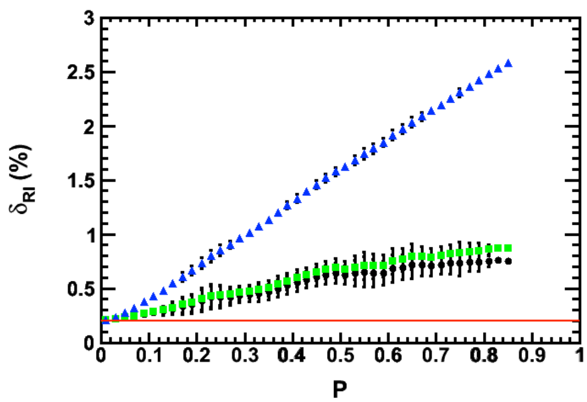

Figure B.2: Uncertainty in the inter-calibrated reflectance as a function of polarization for the 670 nm band derived from the dependence shown in the left plot. The imager sensitivity to polarization was set to 0.03 (approximately MODIS and VIIRS sensitivity) and its relative uncertainty to 10% (third curve from the top, in black), 20% (second curve from the top, in green) and 100% (top curve, in blue). Also shown (bottom line, red) is the uncertainty in reflectance if the polarization is assumed to be zero.

In conclusion, CLARREO's inter-calibration approach in reflected solar may be tested using the empirical Polarization Distribution Models. Such models can be constructed using data from the three polarized channels at 490, 670, and 865 nm of the POLDER instrument aboard the PARASOL satellite. The PDMs may be broken down or combined by different scene types, such as clear-sky ocean, clear-sky vegetation, and deserts, as well as different types of cloudy scenes, such as ice or water clouds. Using radiative transfer modeling, the PDM's coverage can also be extended to the entire visible spectrum.

B. Theoretical Polarization Distribution Models

In *Sun and Lukashin* [2013], the authors employed the adding-doubling method [*Hansen and Hovenier*, 1971, *Evans and Stephens*, 1991], and coupled it with a rough-ocean-surface light reflection matrix [*Cox and Munk*, 1956], to model the reflected solar radiation from the ocean-atmosphere system. This adding-doubling radiative transfer model (ADRTM) outputs are far more accurate than the widely validated discrete-ordinate radiative transfer (DISORT) model results [*Stamnes et al.*, 1988, *Sun and Lukashin*, 2013, *Lacis et al.*, 1998].

We also validated the ADRTM results with the PARASOL [*Tanré et al.*, 2011] polarization measurements as displayed in Figure B.3 [*Sun et al.*, 2015a]. The PARASOL data used is from the 24-day measurements for a wind speed range of 6 to 9 m/s. In the modeling, the wind speed is 7 m/s, the sea-salt AOD is 0.06 at the wavelength of 670 nm, and the US standard atmosphere is used. We also incorporate a thin layer of undetected cirrus cloud with an optical depth of 0.18 in the ADRTM. We only show the data at the relative azimuth

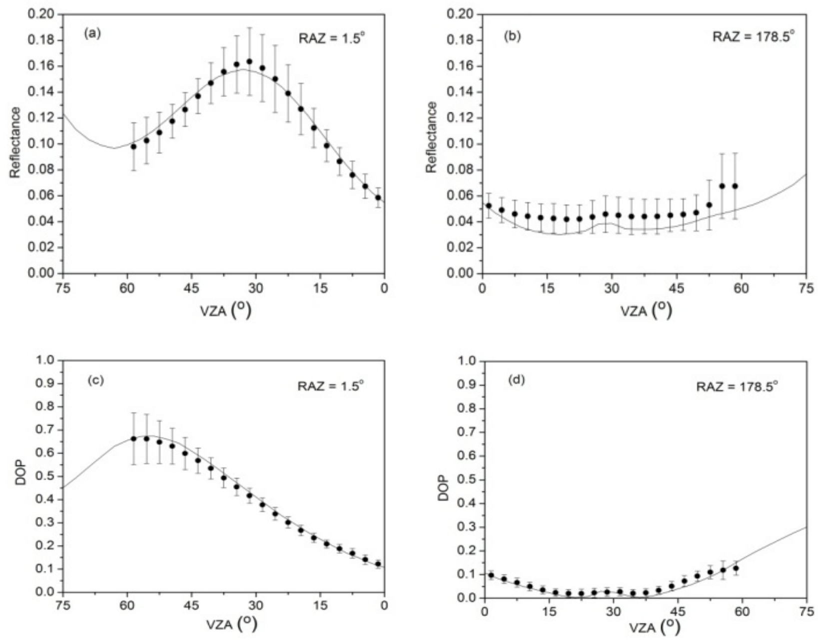

Figure B.3: Directional irradiance reflectance and degree of polarization (DOP), as functions of viewing zenith angle (VZA), at a wavelength of 670 nm from PARASOL data for clear-sky oceans averaged in a solar zenith angle (SZA) bin of 27° – 30° (black dots) and ADRTM results at a SZA of 28.5° (solid curve). Error bars show the standard deviations of the PARASOL data.

angle (RAZ) of 1.5° and 178.5°, respectively. We can see that the reflectance and degree of polarization (DOP) from the PARASOL data and the ADRTM model are in good agreement. We have demonstrated that the angle of linear polarization values from the PARASOL observations and the ADRTM are in very good agreement [*Sun et al.*, 2015a].

We also conducted the validation of the ADRTM for cloud scenes. Good agreement between model results and satellite data is shown for both liquid water clouds and ice clouds [*Sun et al.*, 2014]. Sensitivities of reflected solar radiation's polarization to various ocean-surface and atmospheric conditions are addressed [*Sun and Lukashin*, 2013] and polarization features of desert surfaces in [*Sun et al.*, 2015b]. These studies suggest that the modeling can provide a reliable approach for making the spectral PDM's for CLARREO inter-calibration applications, which cannot be achieved by empirical PDMs alone because of limited spectral coverage.

C Appendix: List of Acronyms

ADRTM – Adding Doubling Radiative Transfer Model
ACCESS – Advancing Collaborative Connections for Earth System Science
ADbS – Absolute Detector-based Source
AVHRR – Advanced Very High Resolution Radiometer BRDF – Bidirectional Reflectance Distribution Function
CCD – Charge-Coupled Device
CDS – Calibration Demonstration System
CERES – Clouds and Earth's Radiant Energy System
CLARREO – Climate Absolute Radiance and Refractivity Observatory
CPF – CLARREO Pathfinder
CMIP3 – Coupled Model Intercomparison Project
CRF – Cloud Radiative Forcing
CXR – CLARREO Transfer Radiometer
DISORT – Discrete Ordinate Radiative Transfer Model
DOP – Degree of Polarization
ELC – ExPRESS Logistics Carrier
ExPRESS – EXpedite the PRocessing of Experiments to Space Station
ENSO – El Niño Southern Oscillation
ESTO – Earth Science Technology Office
FOV – Field-Of-View
FWHM – Full-Width Half-Maximum
GEO – Geostationary Earth Orbit
GFOV – Ground Field Of View
GNSS – Global Navigation Satellite System
GOES – Geostationary Operational Environmental Satellite
GSFC – NASA Goddard Space Flight Center
GSICS – Global Space-based Inter-Calibration System
HIP – Hyperspectral Image Projector
HySICS – Hyperspectral Imager for Climate Science
IFOV – Instantaneous Field Of View
IIP – Instrument Incubator Program
IPCC – Intergovernmental Panel on Climate Change
IR – InfraRed (wavelength range)
ISS – International Space Station
JPSS-1 – Joint Polar Satellite System
LaRC – NASA Langley Research Center
LEO – Low Earth Orbit
MCR – Mission Concept Review
MIIC – Multi-Instrument Inter-Calibration (framework)
MODIS – Moderate Resolution Imaging Spectroradiometer
NIST – National Institute of Standards
OSSE – Observing System Simulation Experiment

PARASOL – Polarization & Anisotropy of Reflectances for Atmospheric Sciences coupled with Observations from a Lidar
PDM – Polarization Distribution Model
POLDER – Polarization and Directionality of Earth's Reflectances
POWR – Primary Optical Watt Radiometer
RBI – Radiation Budget Instrument
RO – Radio Occultation
ROIC – Read-Out Integrated Circuits
ROLO – USGS Robotic Lunar Observatory Irradiance Model
ROSES – Research Opportunities in Space and Earth Science
RS – Reflected Solar
SCIAMACHY – SCanning Imaging Absorption SpectroMeter for Atmospheric CartograpHY
SeaWIFS – Sea-Viewing Wide-Field-of-View Sensor
SI – International System of Units (Système International)
SIRCUS – NISTS's Spectral Irradiance and Radiance Calibrations with Uniform Sources
SMD – NASA's Science Mission Directorate
SNPP – Suomi National Polar-orbiting Partnership named after Verner Suomi
SNO – Simultaneous Nadir Overpass
SNR – Signal to Noise Ratio
SOLARIS – SOlar, Lunar for Absolute Reflectance Imaging Spectroradiometer
SVM – Science Value Matrix
SW – Shortwave
TLE – Two Line Element
TLM – Telemetry
TOA – Top of the Atmosphere
TSIS – Total Solar Irradiance Spectrometer
USGS – United States Geological Survey
VIIRS – Visible Infrared Imaging Radiometer Suite
WASP – Wallops Arc Second Pointer